AD-A161 400 INVESTIGATION OF PLANAR WAVEGUIDES AND COMPONENTS FOR MILLIMETER-WAVE INT..(U) ILLINOIS UNIV AT URBANA COORDINATED SCIENCE LAB K J WEBB ET AL. MAR 85 R-1034 1/1

UNCLASSIFIED N00014-84-C-0149 F/G 9/5 NL

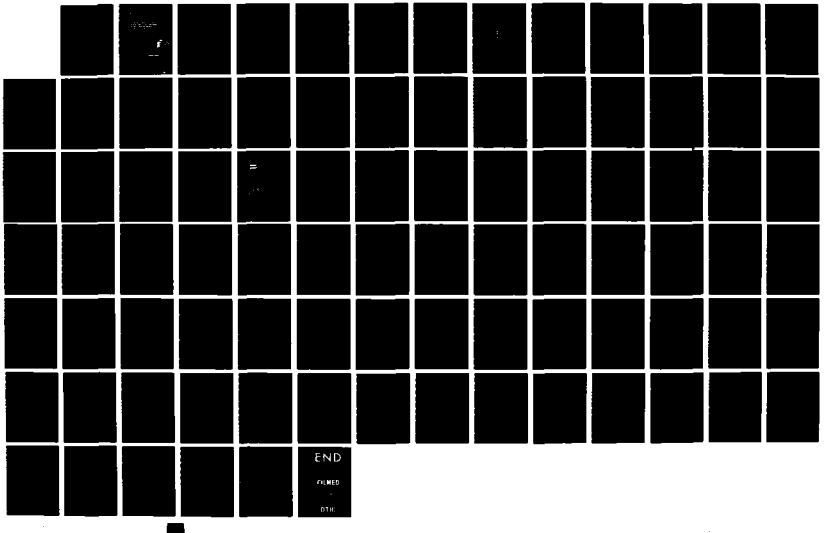

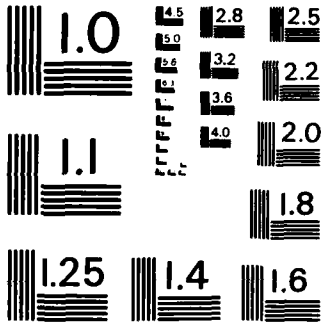

REPORT R-1034 MARCH 1985 (12) UILU-ENG 85-2209

COORDINATED SCIENCE LABORATORY

INVESTIGATION OF PLANAR WAVEGUIDES AND COMPONENTS FOR MILLIMETER-WAVE INTEGRATED CIRCUITS

K. J. WEBB
R. MITTRA

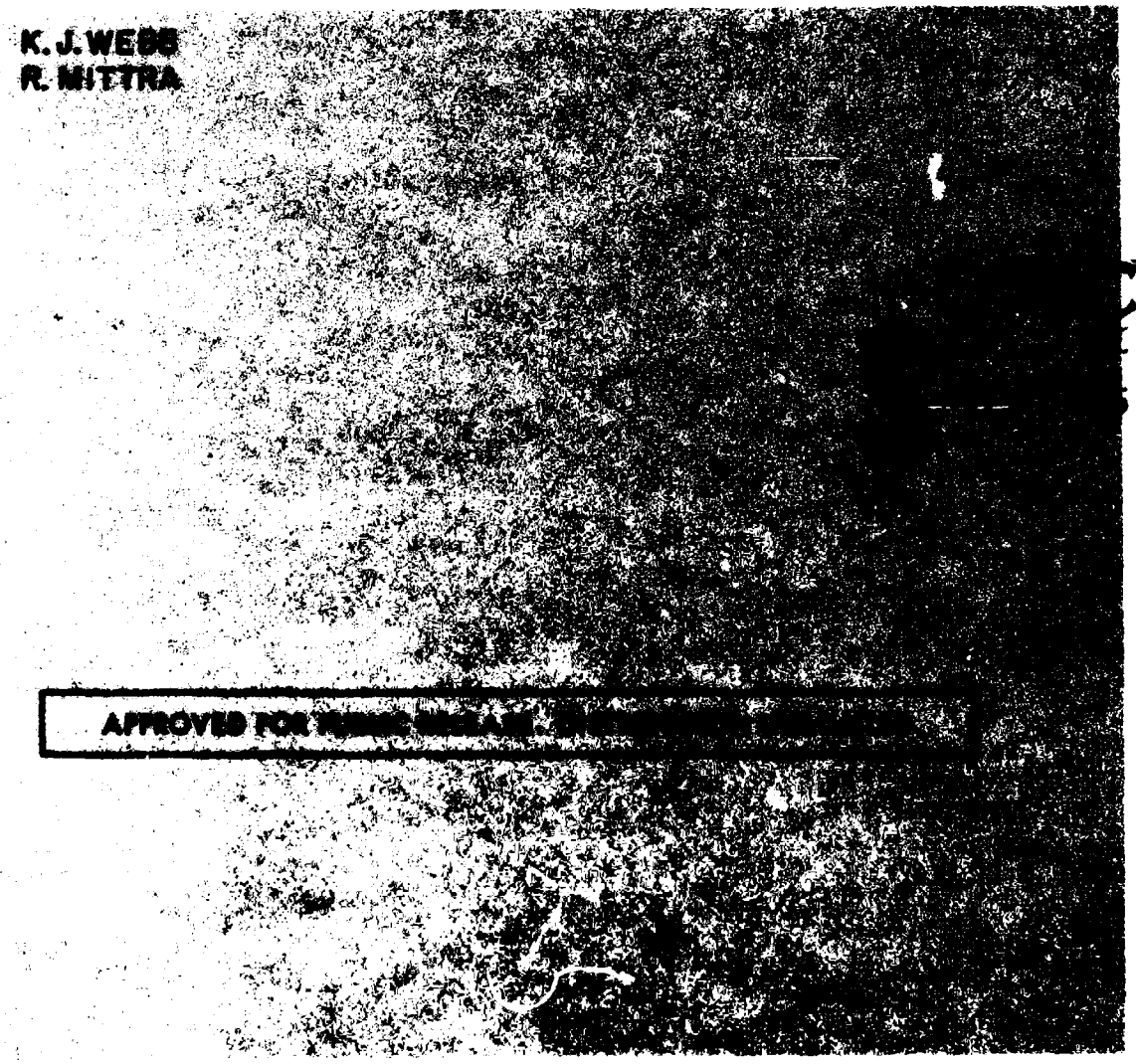

UNIVERSITY OF ILLINOIS - URBANA, ILLINOIS

REPORT DOCUMENTATION PAGE

1a. REPORT SECURITY CLASSIFICATION Unclassified	1b. RESTRICTIVE MARKINGS None
2a. SECURITY CLASSIFICATION AUTHORITY N/A	3. DISTRIBUTION/AVAILABILITY OF REPORT Approved for public release, distribution unlimited.
2b. DECLASSIFICATION/DOWNGRADING SCHEDULE N/A	
4. PERFORMING ORGANIZATION REPORT NUMBER(S) R-report #1034	5. MONITORING ORGANIZATION REPORT NUMBER(S) N/A
6a. NAME OF PERFORMING ORGANIZATION Coordinated Science Lab. Univ. of Illinois	6b. OFFICE SYMBOL (If applicable) N/A
	7a. NAME OF MONITORING ORGANIZATION Office of Naval Research
6c. ADDRESS (City, State and ZIP Code) 1101 W. Springfield Avenue Urbana, Illinois 61801	7b. ADDRESS (City, State and ZIP Code) 800 N. Quincy Street Arlington, VA 22217
8a. NAME OF FUNDING/SPONSORING ORGANIZATION	8b. OFFICE SYMBOL (If applicable) N/A
	9. PROCUREMENT INSTRUMENT IDENTIFICATION NUMBER Contract #N00014-84-C-0149
8c. ADDRESS (City, State and ZIP Code)	10. SOURCE OF FUNDING NOS.

PROGRAM ELEMENT NO.	PROJECT NO.	TASK NO.	WORK UNIT NO.

11 TITLE (Include Security Classification)
Investigation of Planar Waveguides & Components for Millimeter-Wave Integrated Circuits

12. PERSONAL AUTHOR(S)
K. J. Webb and R. Mittra

13a. TYPE OF REPORT	13b. TIME COVERED	14. DATE OF REPORT (Yr., Mo., Day)	15. PAGE COUNT
Technical	FROM _____ TO _____	March 1985	83

16. SUPPLEMENTARY NOTATION
N/A

17. COSATI CODES			18. SUBJECT TERMS (Continue on reverse if necessary and identify by block number)
FIELD	GROUP	SUB. GR.	Millimeter Waves; Integrated Circuits; Numerical Techniques

19. ABSTRACT (Continue on reverse if necessary and identify by block number)

Several important elements in millimeter-wave integrated circuit systems are studied. Filter-type structures which are composed of a series of discontinuities are employed frequently in such systems. The study of the general discontinuity problem is thus very important.

20. DISTRIBUTION/AVAILABILITY OF ABSTRACT UNCLASSIFIED/UNLIMITED ☒ SAME AS RPT. ☐ DTIC USERS ☐	21. ABSTRACT SECURITY CLASSIFICATION Unclassified

22a. NAME OF RESPONSIBLE INDIVIDUAL	22b. TELEPHONE NUMBER (Include Area Code)	22c. OFFICE SYMBOL
		None

INVESTIGATION OF PLANAR WAVEGUIDES AND COMPONENTS FOR MILLIMETER-WAVE INTEGRATED CIRCUITS

K. J. Webb and R. Mittra

Department of Electrical & Computer Engineering
University of Illinois
Urbana, Illinois

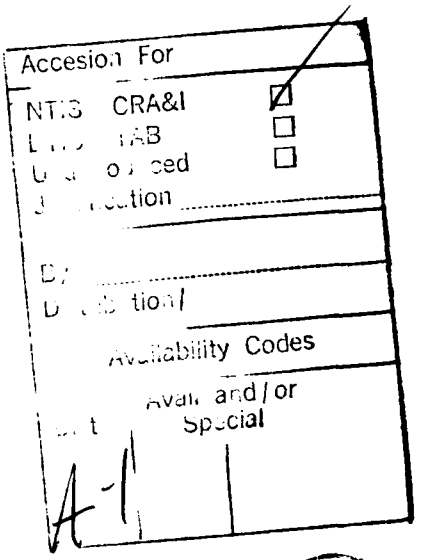

The work reported in this paper was supported in part by the Joint Services Electronics Program, N00014-84-C-0149.

TABLE OF CONTENTS

Chapter 1: INTRODUCTION

Millimeter-wave systems have received increased interest in recent years, and serve a broad spectrum of applications. Many of these systems employ receiver and transmitter sub-systems. The use of integrated circuits at millimeter-wave frequencies is essential to meet performance, cost, size, and other constraints. The integration of millimeter-wave transmitters and receivers is of primary importance. It is desirable to place as many components as possible; for example, amplifiers, filters, switches, antennas; on one substrate or waveguide medium. Millimeter-wave integrated circuits are receiving considerable exposure [1], [2].

This thesis considers several important elements for use in millimeter-wave integrated circuits. Two different wave-guiding media are considered: fin-line, which is a member of the metallized substrate family, and image guide, which is a member of the rectangular dielectric waveguide family.

Filter-type structures, which consist of a series of discontinuities, are studied. These structures are used in matching elements for active devices and antennas, radiating elements, and as filters. Some of these components have been studied [3]-[7].

The solution of the discontinuity problem is therefore of particular importance. A suitable characterization for a single discontinuity permits the analysis of some series of discontinuities via generalized scattering and transmission matrices.

The uniform fin-line structure is analyzed in Chapter 2. This analysis gives propagation constants, characteristic impedances and mode functions.

Chapters 3 and 4 deal with two different approaches for solving the fin-line discontinuity problem. A moment method is used to study a single and an infinite periodic array of discontinuities in Chapter 3. An iterative method and a variational approach are used to solve the single fin-line discontinuity problem in Chapter 4.

An image guide grating filter is studied in Chapter 5. Theoretical and experimental curves for the insertion loss characteristic are given.

CHAPTER 2: UNIFORM FIN-LINE ANALYSIS

2.1. Introduction

The unilateral fin-line structure shown in Fig. 2.1. is studied in this thesis. It consists of a metal cladding on one side of a dielectric substrate, which is mounted in a shielded enclosure. The metallization will be assumed infinitesimally thin. A generalized guide may consist of some combination of dielectrics and metallized surfaces.

A number of recent papers have used the spectral domain formulation, in conjunction with a moment method, to analyze the fin-line [8]-[12]. In particular, Galerkin's method has been shown to be satisfactory.

Several of these authors have analyzed the fin-line structure by expressing the fields in terms of scalar potential functions in each transverse region, and then applying the appropriate boundary conditions to obtain the required coupled equations [8], [9], [11]. This approach is satisfactory when the structure can be analyzed as a two-region problem, for example, symmetric bilateral fin-line. However, the unilateral fin-line is a three-region problem, which results in prohibitive algebra. For a larger number of regions the problem is compounded.

An alternative approach is to use the transverse resonance technique in the spectral domain [10], [12]. This method greatly simplifies the formulation, and will be utilized in the work presented here.

The uniform fin-line problem is formulated in Section 2.2. Details of the formulation procedure and the numerical methods used in the solution, namely, the moment method, are given. It is necessary to obtain data for the propagation constants, characteristic impedances and the mode functions. Theoretical and experimental results are given in Section 2.3.

2.2. Spectral Domain Formulation for Fin-Line

Waveguides such as fin-line and microstrip are most simply formulated in the spectral domain. This involves using the Fourier series representation of all field quantities in the transverse direction,

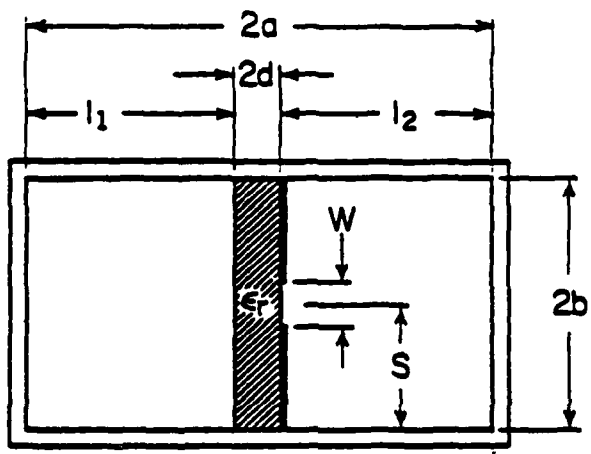

Figure 2.1. Unilateral fin-line structure.

parallel to the metallization. This is the x-direction for the geometry of Fig. 2.1. The transform pair for quantity A is defined as

$$\tilde{A}(k_x,y) = \frac{1}{2b}\int_0^{2b} A(x,y)\, e^{jk_x x}\, dx \tag{2.1a}$$

$$A(x,y)e^{-jk_z z} = \sum_{n=-\infty}^{\infty} \tilde{A}(k_x,y)\, e^{-j(k_x x + k_z z)} \tag{2.1b}$$

$$\text{where} \quad k_x = \frac{2n\pi}{2b},\ n = 0, \pm 1, \pm 2,\ldots$$

The continuous Fourier Transform may be used to find these quantities at the discrete k_x values.

Without the metallization on the dielectric surface, TE-to-y and TM-to-y modes propagate. The fin-line modes can be considered as superpositions of these modes.

An analogy is now drawn with a plane wave incident on a dielectric boundary at some angle. If the fields are decomposed into components parallel and perpendicular to the propagation direction, no coupling between these components will occur at the interface. The resulting equations have been decoupled.

A similar concept may be employed in the fin-line case. Equation (2.1b) represents a superposition of plane waves propagating in the $(k_x x + k_z z)$ direction, which will be called the u-direction. Consider the orthogonal (u,v) coordinate system in the (x,z) plane, as shown in Fig. 2.2(a). The following coordinate transformation relationships hold for quantity a

$$a_u = a_z\, N_z + a_x\, N_x \tag{2.2a}$$

$$a_v = -a_z\, N_x + a_x\, N_z$$

$$a_z = a_u\, N_x + a_v\, N_z \tag{2.2b}$$

$$a_z = a_u\, N_z - a_v\, N_x$$

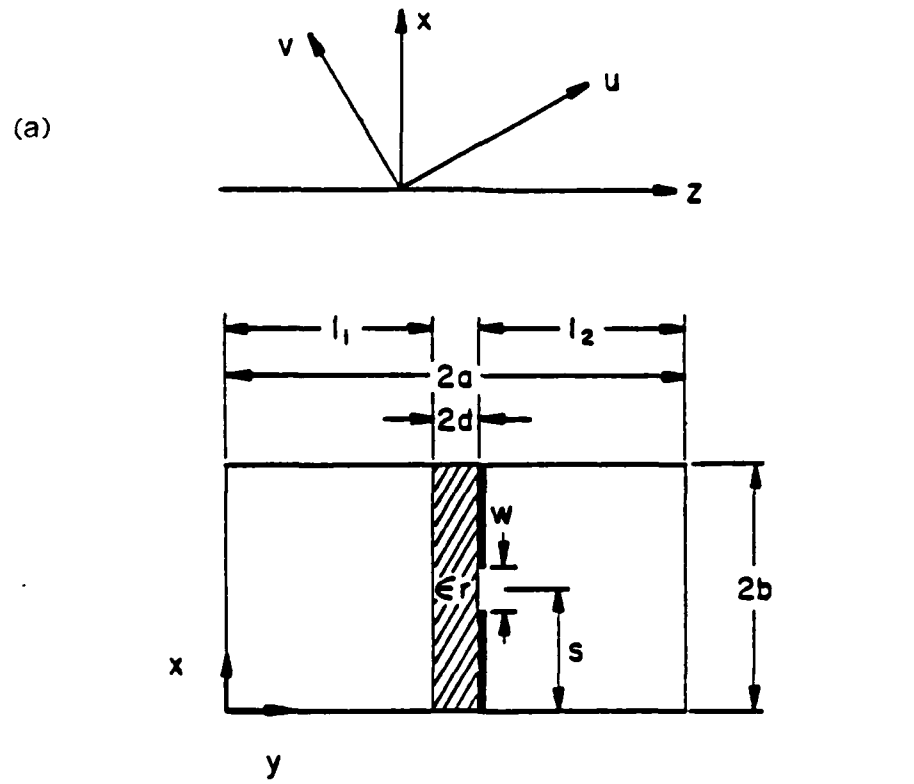

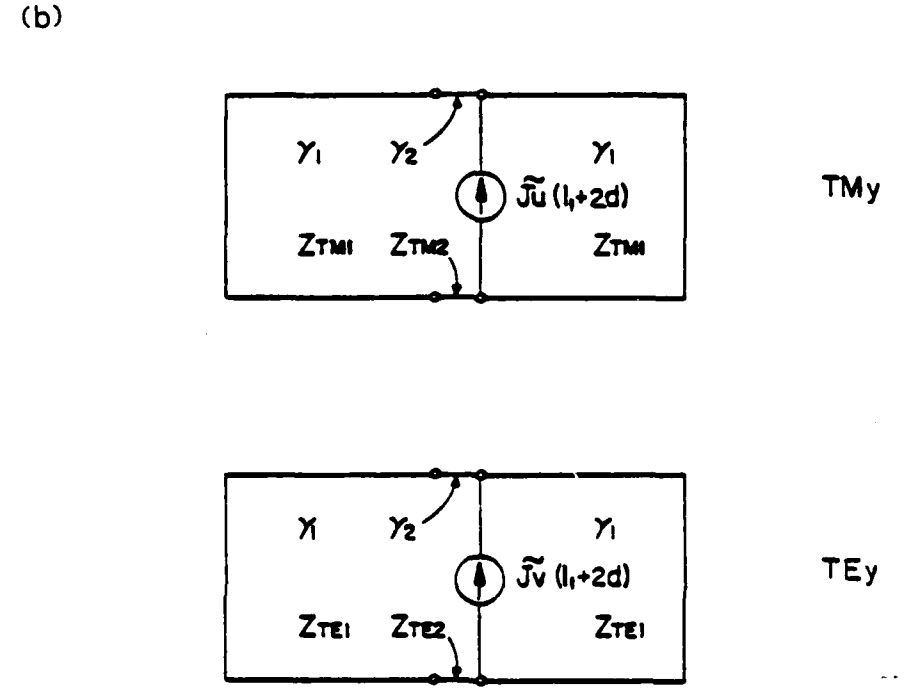

Figure 2.2. (a) (x,z) and (u,v) coordinate system, (b) Equivalent transverse resonance circuits for analyzing the fin-line structure.

$$\left.\begin{aligned} N_x &= \frac{k_x}{\sqrt{k_x^2 + k_z^2}} \\ N_z &= \frac{k_z}{\sqrt{k_x^2 + k_z^2}} \end{aligned}\right\} \tag{2.3}$$

The field quantities expressed in the (u,v) coordinate system allow a decoupled transverse resonance analysis. The two equivalent transmission lines for TM to y and u ($\tilde{E}_y, \tilde{E}_u, \tilde{H}_v$) and TE to y and u ($\tilde{H}_y, \tilde{E}_v, \tilde{H}_u$) are shown in Fig. 2.2(b). The wave impedances in the y-direction are

$$\left.\begin{aligned} Z_{TMi} &= \frac{\tilde{E}_{ui}}{H_{vi}} = \frac{\gamma_i}{j\omega\epsilon_o\epsilon_{ri}} \\ Z_{TEi} &= \frac{-\tilde{E}_{vi}}{H_{ui}} = \frac{j\omega\mu}{\gamma_i} \end{aligned}\right\} \tag{2.4}$$

where $\gamma_i = \sqrt{k_x^2 + k_z^2 - \epsilon_o\epsilon_{ri}k_o^2}$.

Spectral domain relationships between the fin current densities and the slot fields may be formed simply from the transmission line equivalent circuits. The relationships are

$$\tilde{J}_u(k_x l_1 + 2d) = Y_m \tilde{E}_u(k_x l_1 + 2d) \tag{2.5a}$$

$$\tilde{J}_v(k_x l_1 + 2d) = Y_e \tilde{E}_v(k_x l_1 + 2d) \tag{2.5b}$$

where
$$Y_m = \frac{1}{Z_{TM2}\tanh(\gamma_2 l_2)} + \frac{Z_{TM1} + Z_{TM2}\tanh(\gamma_2 l_1)\tanh({}_2\gamma_1 d)}{Z_{TM1}(Z_{TM2}\tanh(\gamma_2 l_1) + Z_{TM1}\tanh({}_2\gamma_1 d))}$$

$$Y_e = \frac{1}{Z_{TM2}\tanh(\gamma_2 l_2)} + \frac{Z_{TE1} + Z_{TE2}\tanh(\gamma_2 l_1)\tanh({}_2\gamma_1 d)}{Z_{TE1}(Z_{TE2}\tanh(\gamma_2 l_1) + Z_{TE1}\tanh({}_2\gamma_1 d))}.$$

Transformation of Eq. (2.5) back into (x,z) coordinates results in two coupled equations, which are

$$\tilde{J}_x(k_x l_2 + 2d) = (N_x^2 Y_m + N_z^2 Y_e)\tilde{E}_x(k_x l_1 + 2d) + N_x N_z (Y_m - Y_e)\tilde{E}_z(k_x l_1 + 2d) \tag{2.6a}$$

$$\tilde{J}_z(k_x l_1 + 2d) = N_x N_z (Y_m - Y_e)\tilde{E}_x(k_x l_1 + 2d) + (N_z^2 Y_m + N_x^2 Y_e)\tilde{E}_z(k_x l_1 + 2d). \tag{2.6b}$$

Equation (2.6) is a spectral domain relationship between the fin currents and the slot fields. This may be written in the form

$$\begin{bmatrix} Y_{xx} & Y_{xz} \\ Y_{zx} & Y_{zz} \end{bmatrix} \begin{bmatrix} \tilde{E}_x \\ \tilde{E}_z \end{bmatrix} = \begin{bmatrix} \tilde{J}_x \\ \tilde{J}_z \end{bmatrix} \tag{2.7}$$

where the Y-matrix is a type of dyadic Green's function. Only minor alterations to the transmission line equivalent circuits are required to analyze an arbitrary number of dielectric layers and metallized surfaces.

The moment method may be used to obtain a satisfactory numerical solution to Eq. (2.6). A matrix equation may be obtained by the application of Galerkin's method (testing functions being the same as the basis functions) to Eq. (2.6). The slot fields are expanded in terms of a suitable set of basis functions, which satisfy the edge condition, and are readily Fourier transformable. The representation with P basis functions is

$$E_x(x) = \sum_{p=1}^{P} a_p \, \zeta_p(x) \tag{2.8a}$$

$$E_z(x) = \sum_{q=1}^{Q} b_q \, \eta_q(x). \tag{2.8b}$$

A suitable set of functions is an orthogonal polynomial set, modified by the edge condition. The functions used are

$$\left.\begin{aligned} \zeta_p(x) &= \frac{\cos\left[\frac{(p-1)\pi}{w}(x-s-\frac{w}{2})\right]}{\sqrt{1-\left|\frac{2(x-s)}{w}\right|^2}}, \; p = 1,2,3,\ldots \\ \eta_q(x) &= \frac{\sin\left[\frac{q\pi}{w}(x-s-\frac{w}{2})\right]}{\sqrt{1-\left|\frac{2(x-s)}{w}\right|^2}}, \; q = 1,2,3,\ldots \end{aligned}\right\} \; s-\frac{w}{2} < x < s+\frac{w}{2} \tag{2.9}$$

$$\left.\begin{aligned} \zeta_p(x) &= 0 \\ \eta_z(x) &= 0 \end{aligned}\right\} \textit{otherwise.}$$

Frequently, $\zeta_o(x) = P_s(s,w)$ is used. These functions are shown in Fig. 2.3 and Fig. 2.4.

For a centrally located slot, only even ζ and odd η terms (with respect to the center of the slot) are required, i.e., p=0,2,4,... q=2,4,6,... .

The matrix equation is formed using the inner product.

$$<\tilde{X}_i(k_x),\tilde{Y}_j(k_x)> = \sum_{n=-\infty}^{\infty} \tilde{X}_i^*(k_x)\tilde{Y}_j(k_x) \tag{2.10}$$

$$\text{where} \quad k_x = \frac{2n\pi}{2b}.$$

Of course, the summation must be truncated to a finite number of terms. The resulting homogeneous equation is of the form

$$[A]\,[x] = 0. \tag{2.11}$$

For P E_x basis functions and Q E_z basis functions, A is a (P+Q, P+Q) matrix and x a (P+Q,1) vector containing the unknown basis function coefficients. The eigenvalue solutions for k_z are found by solving det (A) = 0. The coefficient matrix x may then be found. P+Q-1 unknowns may be found in terms of one unknown. Thus the approximate E_x and E_z eigenfunctions in the slot can be found. The fields over the complete waveguide cross-section, and hence the mode functions, may be found by returning to the equivalent transverse resonance circuits.

There is no unique definition for the characteristic impedance for non-TEM modes. A suitable definition as discussed in [10], [13] is

$$Z_o = \frac{|V_x|^2}{2P} \tag{2.12}$$

where V_x is the slot voltage and P the mode power. The slot voltage is given by

$$V_x = \int_{s-\frac{w}{2}}^{s+\frac{w}{2}} E_x(x,l_1 + 2d)dx. \tag{2.13}$$

The mode power is given by

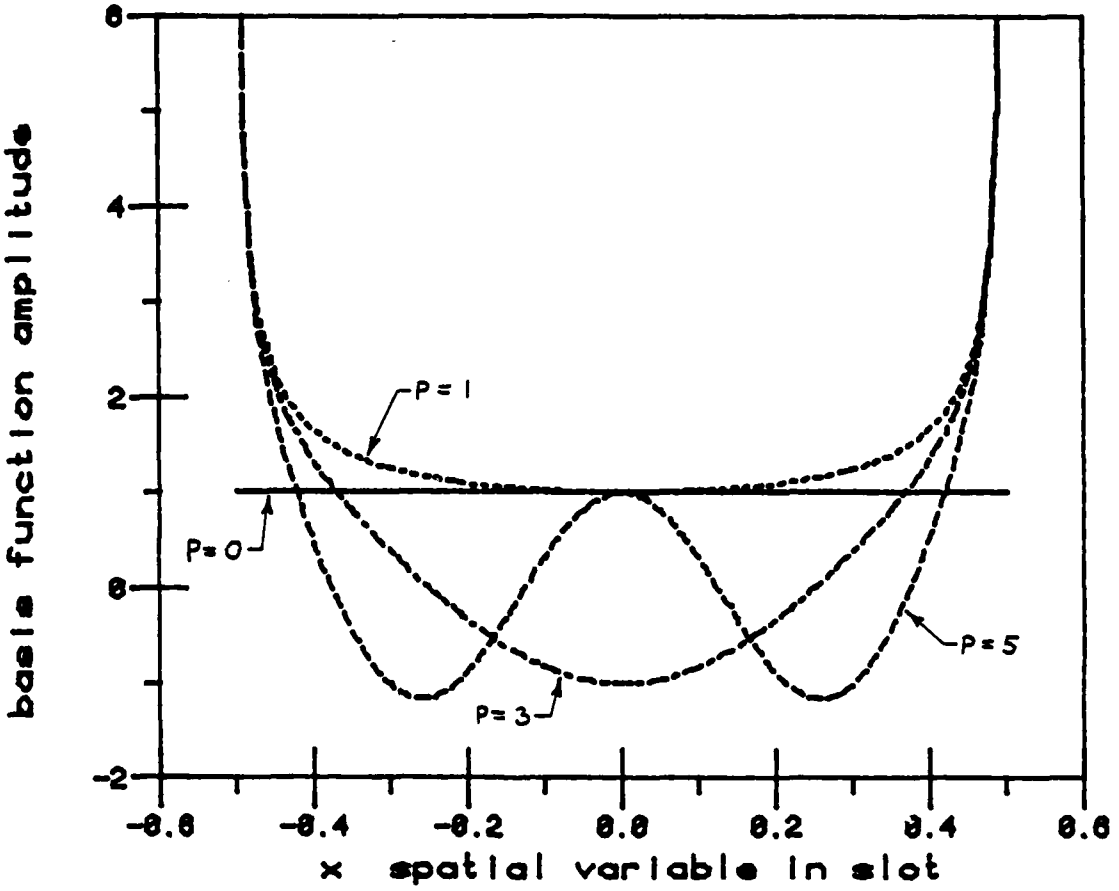

Figure 2.3. Basis functions for $E_z(x)$ in the fin plane.

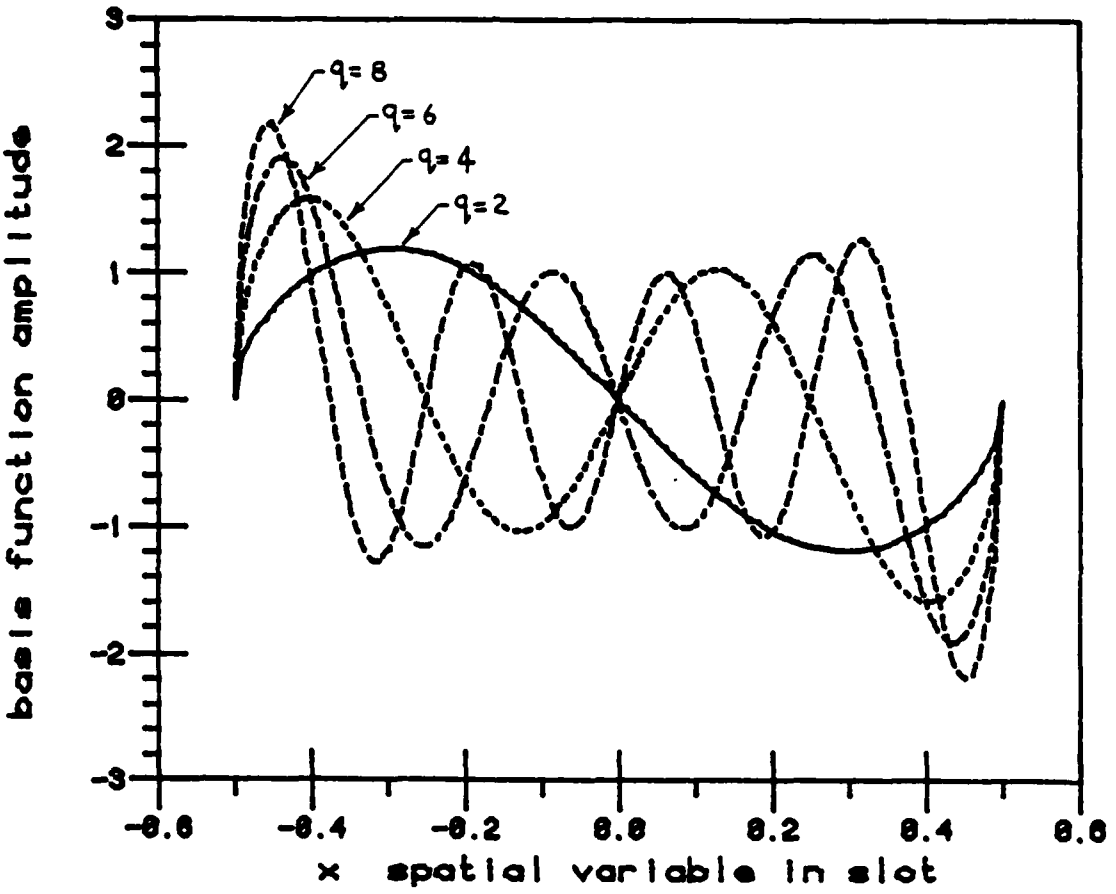

Figure 2.4. Basis functions for $E_z(x)$ in the fin plane.

$$P = \frac{1}{2}\,\mathrm{Re}\left\{\int_0^{2a}\int_0^{2b} E_x(x,y)H_y^*(s,y) - E_y(x,y)H_x^*(x,y)\,dxdy\right\}. \tag{2.14}$$

Using Parseval's theorem, this may be expressed as

$$P = \frac{1}{4b}\,\mathrm{Re}\left\{\sum_{n=-\infty}^{\infty}\int_0^{2a} [\tilde{E}_x(k_x,y)\tilde{H}_y^*(k_x,y) - \tilde{E}_y(k_x,y)\tilde{H}_x^*(k_x,y)]dy\right\}. \tag{2.15}$$

$\tilde{E}_x, \tilde{H}_y, \tilde{E}_y$ and $\tilde{H}_x$ may be found in the (u,v) coordinate system as voltages and currents to the equivalent transmission lines, giving

$$\tilde{E}_x(k_x,y)\tilde{H}_y^*(k_x,y) = \frac{k_z}{\omega\mu}|\tilde{E}_v(k_x,y)|^2 + \frac{k_x}{\omega\mu}\tilde{E}_u(k_x,y)\tilde{E}_v^*(k_x,y) \tag{2.16a}$$

$$\tilde{E}_y(k_x,y)\tilde{H}_x^*(k_x,y) = (\tilde{H}_u^*(k_x,y)N_x + \tilde{H}_v^*(k_x,y)N_z). \tag{2.16b}$$

The y-integrals may be performed analytically. This approach simplifies the computation of the mode power.

The fields for the nth mode may be expressed as

$$\bar{E}(x,y,z) = \bar{e}_n(x,y)e^{-jk_{zn}z} + \bar{e}_{zn}(x,y)e^{-jk_{zn}z} \tag{2.17a}$$

$$\bar{H}(x,y,z) = \bar{h}_n(x,y)e^{-jk_{zn}z} + \bar{h}_{zn}(x,y)e^{-jk_{zn}z} \tag{2.17b}$$

where $\bar{e}_n$ and $\bar{h}_n$ are transverse vector mode functions, and $\bar{e}_{zn}$ and $\bar{h}_{zn}$ are longitudinal vector mode functions. These mode functions, when normalized, satisfy the following orthogonality relation [14]

$$\int_s \int \bar{e}_x \times \bar{h}_m \cdot \hat{z}\,ds = \delta_{nm}$$

where δ_{nm} is the Kronecker data which is defined by

$$\delta_{nm} = \begin{cases} 1 & n = m \\ 0 & n \neq m \end{cases}. \tag{2.18}$$

2.3. Results and Discussion

For the purposes of this study, a centrally located slot will be considered. The techniques presented can be used to analyze an arbitrary number of slots located anywhere in the shielded enclosure.

Satisfactory approximate results for the propagation constant can be obtained by using $E_x = P_x(s,w)$ and $E_z = 0$. Upon investigation of the convergence of the propagation constant solutions, two basis functions from Eq. (2.8) (p=1,3, q=2,4) give sufficient accuracy. A "rule of thumb" for the number of spectral terms required in the inner-product of Eq. (2.9) is

$$\sum_{n=-N/2}^{N/2} \tilde{X}_i^*(k_x)\tilde{Y}_j(k_x) \quad , \quad N \geq \frac{16b}{w} . \tag{2.19}$$

This indicates that more spectral terms are required for a larger waveguide width to slot width ratio. This number of basis functions gives good results without excessive computation time. Eigenvalue solutions to Eq. (2.10) can be found by a course iteration to find approximate solutions, followed by iterations using Newton's method.

The effective dielectric ($\epsilon_{eff} = k_z^2/k_o^2$) constant results agree with Schmidt et al. [10]. A comparison of the computed normalized wavelength with Knorr and Shayda [8] is given in Fig. 2.5. Knorr and Shayda use a pulse approximation for E_x in the slot.

Experimental propagation constants at E-band (76-82 GHz) have been obtained [15]. Figures 2.6 and 2.7 give comparisons between the theory presented here and this experimental data. The agreement is quite good. Additional propagation data, for propagating and evanescent modes, which will be used in subsequent chapters, is presented in Figs. 2.8, 2.9 and 2.10.

The characteristic impedance, as defined by Eq. (2.12), is plotted for several cases in Figs. 2.11 and 2.12. A pulse representation of E_x is used here. Note that the impedance increases with increasing slot width.

The nature of the Green's function matrix $\overline{\overline{Y}}$ is of importance when computing infinite summations and integrals in the spectral domain. The asymptotic form of $\overline{\overline{Y}}$ is particularly important. For

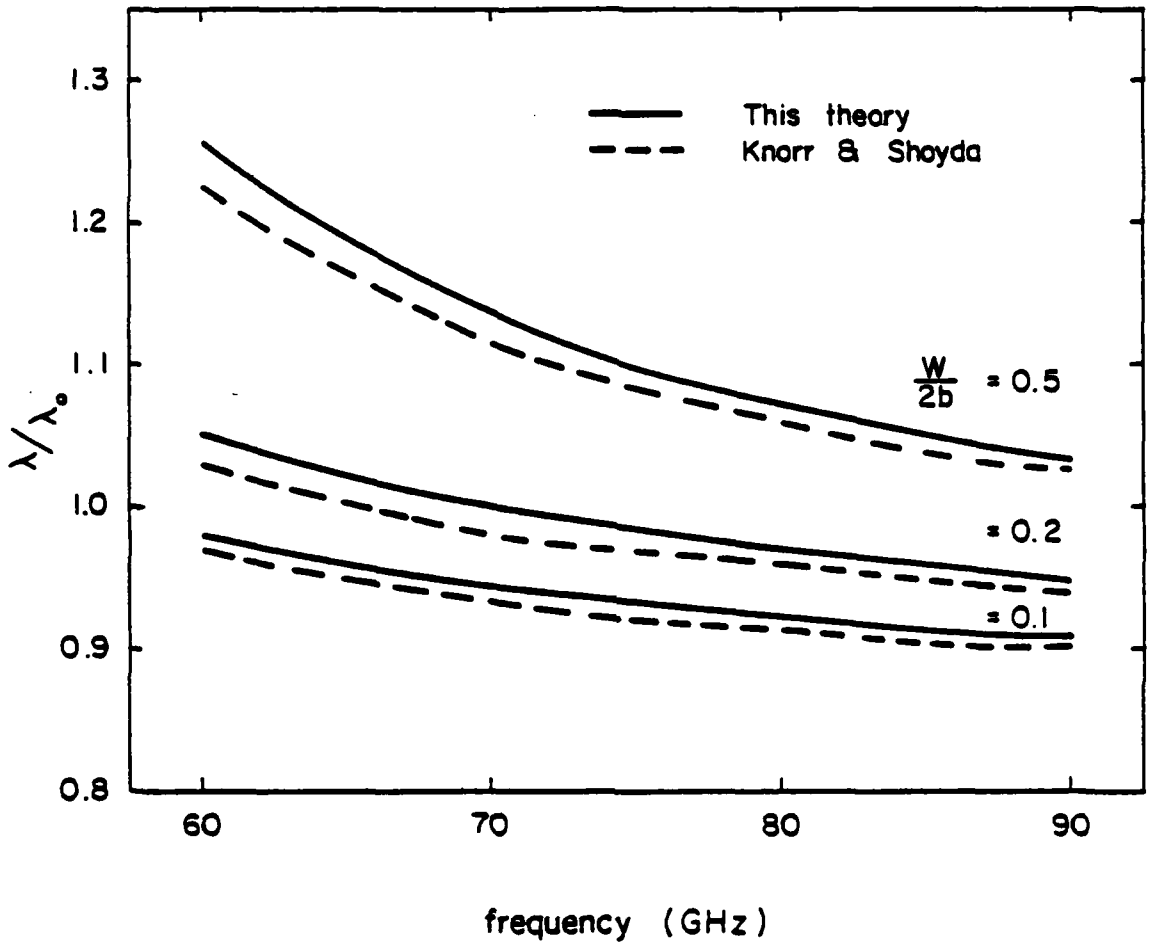

Figure 2.5. Phase constant curves for unilateral fin-line with a WR-12 waveguide shield. $l_1 = 1.422\ mm$, $l_2 = 1.549\ mm$, $2d = 0.254\ mm$, $\epsilon_r = 2.2$, $2b = 2.556\ mm$, $f = 14\ GHz$.

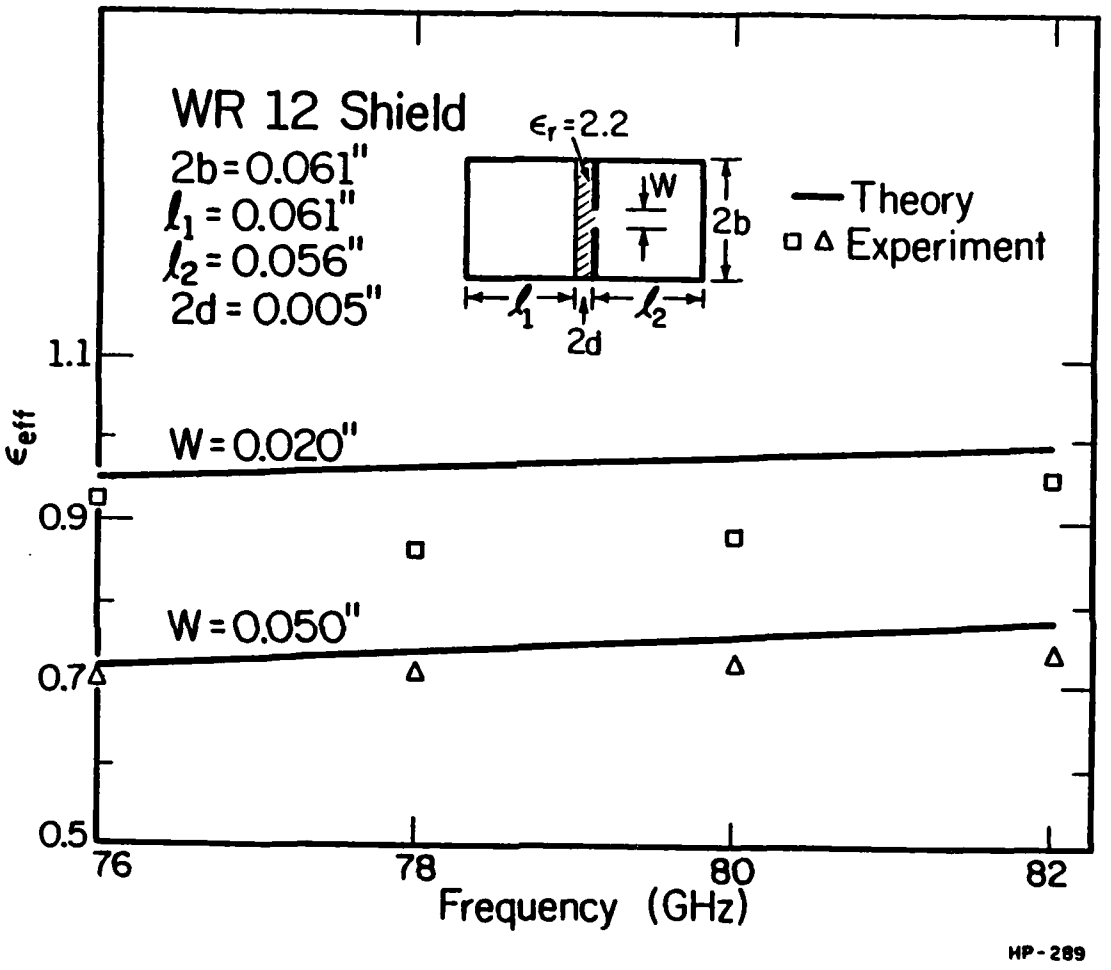

Figure 2.6. Comparison of theoretical and experimental results for the effective dielectric constant of fin-line in a WR-12 shield.

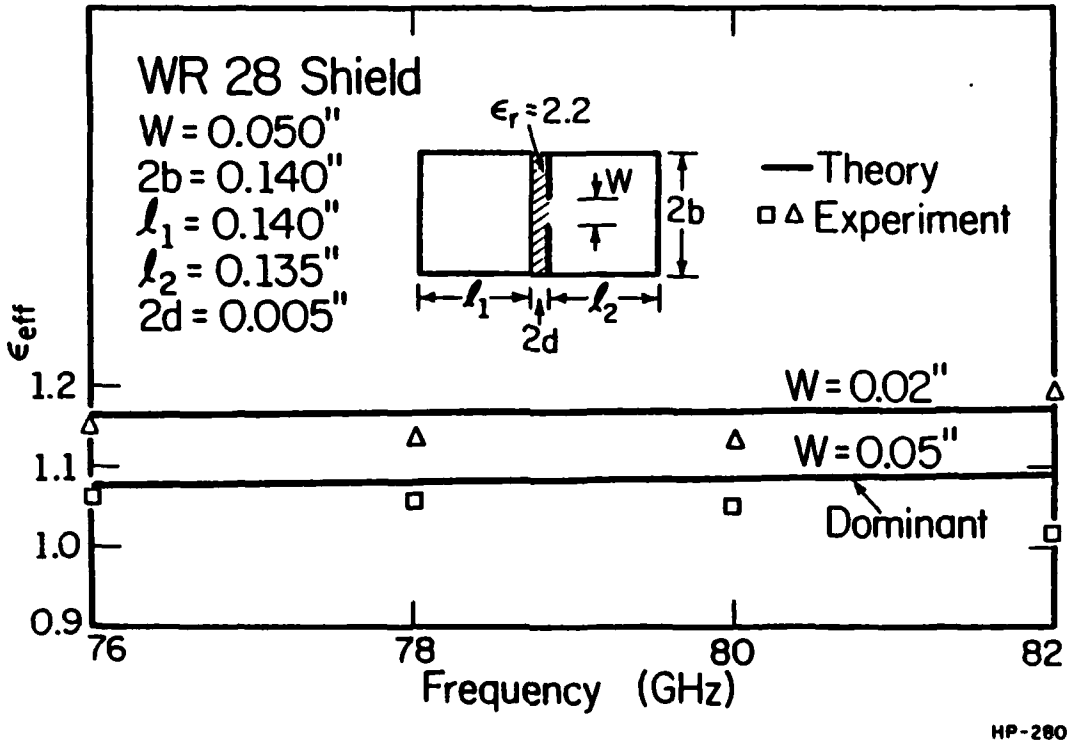

Figure 2.7. Comparison of theoretical and experimental results for the effective dielectric constant of fin-line in a WR-28 shield.

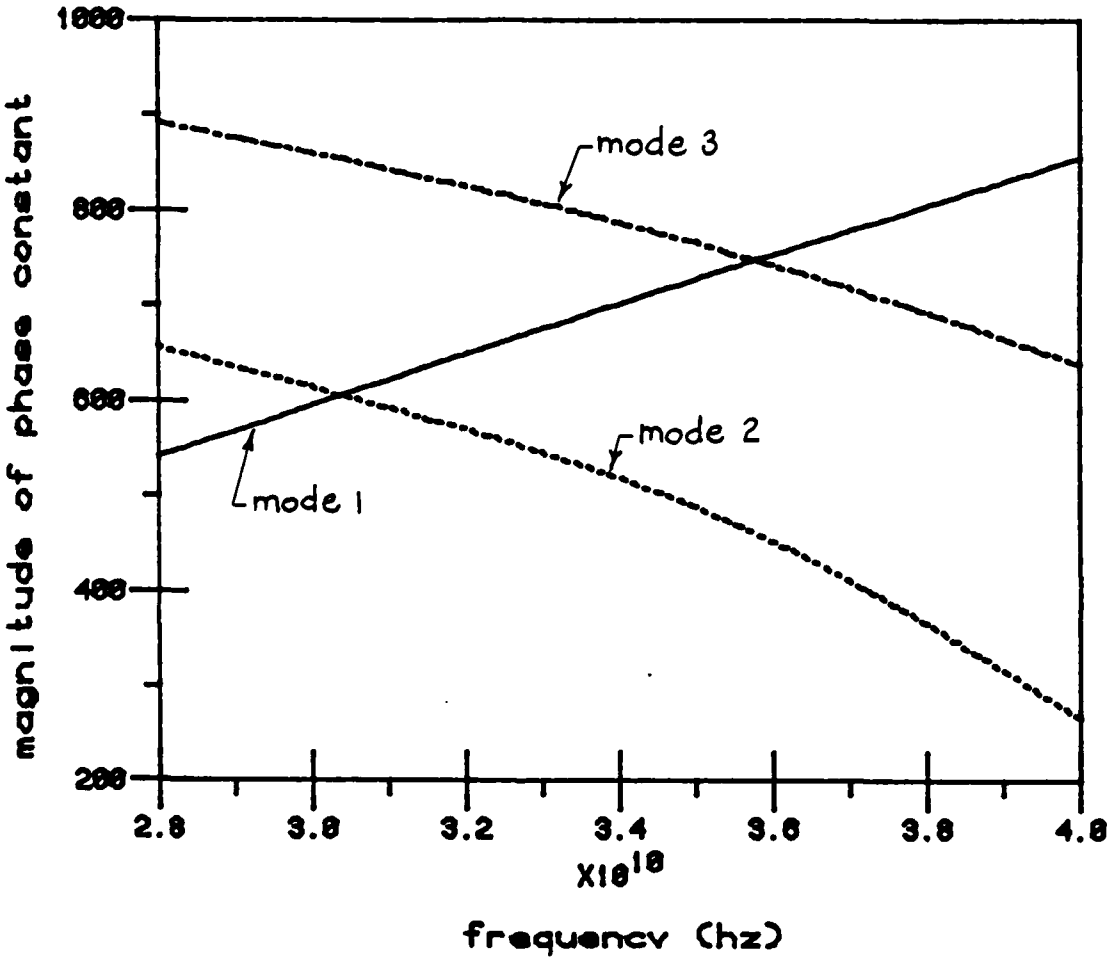

Figure 2.8. Dispersion curves for three even modes (E_x even about $x = s$) in unilateral fin-line with a WR-28 shield. $l_1 = l_2 = 3.429$ *mm*, $2d = 0.254$ *mm*, $\epsilon_r = 2.22$, $2b = 2.556$ *mm*, $w = 1$ *mm*.

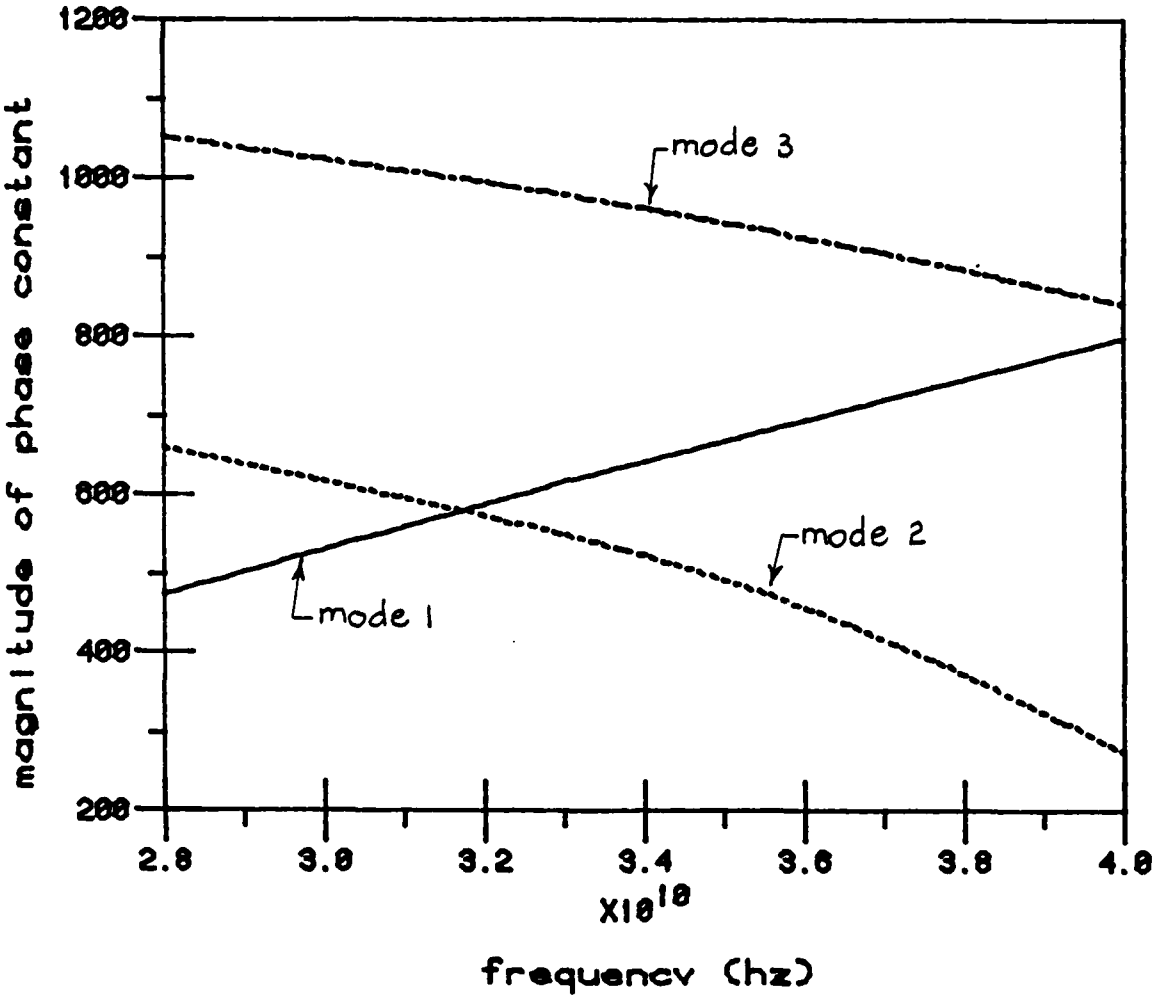

Figure 2.9. Dispersion curves for three even modes (E_x even about $x=s$) in unilateral fin-line with a WR-28 shield. $l_1 = l_2 = 3.429$ *mm*, $2d = 0.254$ *mm*, $\epsilon_r = 2.22$, $2b = 2.556$ *mm*, $w = 2$ *mm*.

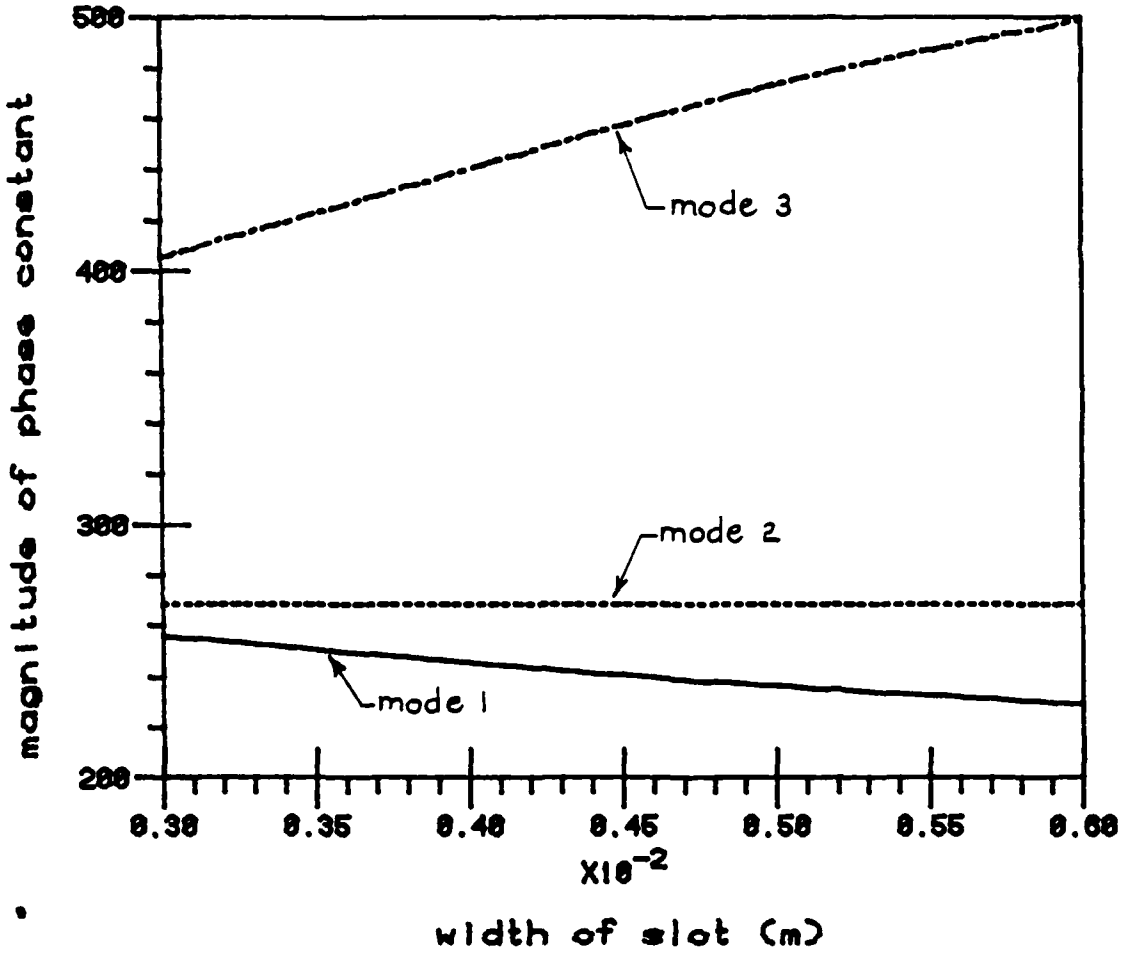

Figure 2.10. Dispersion curves for three even modes (E_x even about $x = s$) in unilateral fin-line with a WR-62 shield. $l_1 = l_2 = 7.773$ *mm*, $2d = 0.254$ *mm*, $\epsilon_r = 2.2$, $2b = 7.9$ *mm*, $f = 14$ GHz.

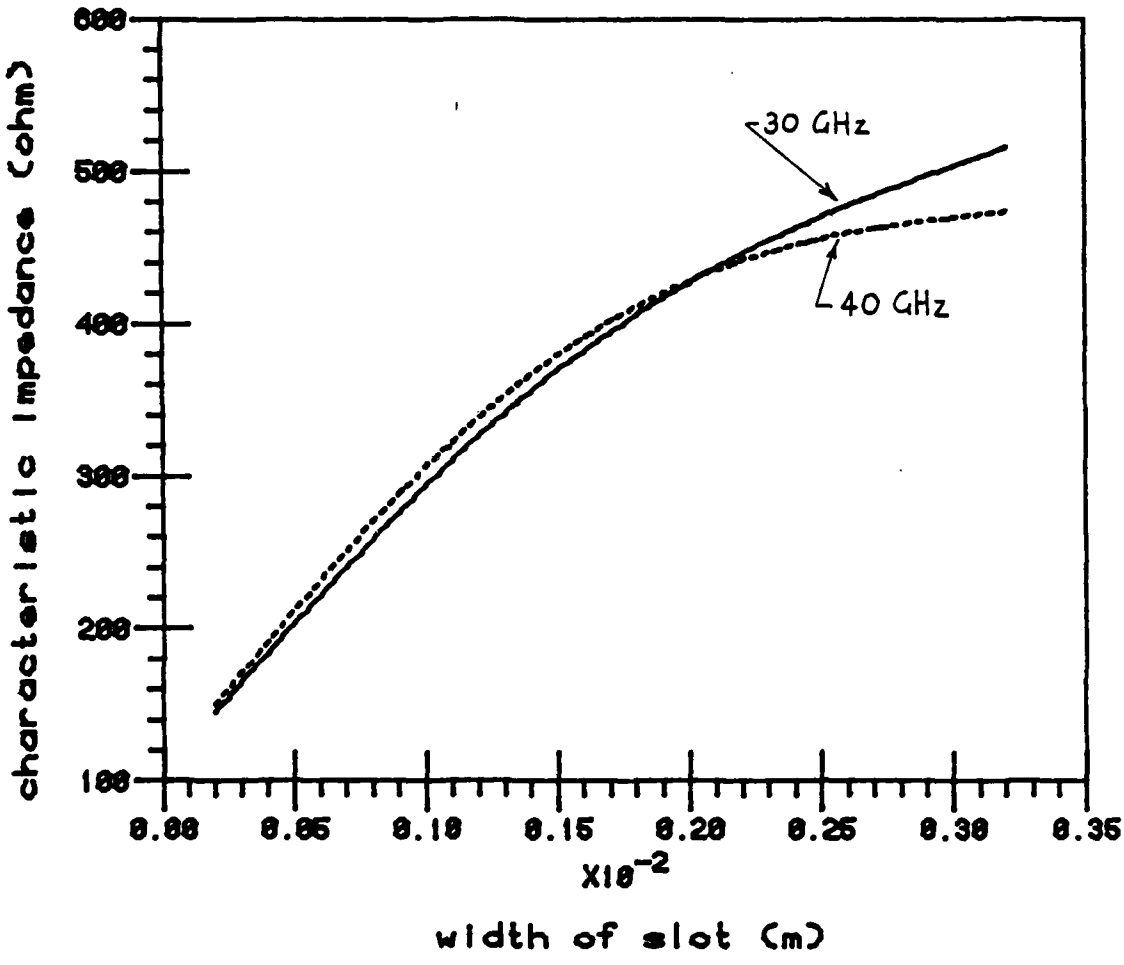

Figure 2.11. Characteristic impedance for fin-line with a WR-28 shield using a pulse approximation for E_x. $l_1 = l_2 = 3.429\ mm$, $2d = 0.254\ mm$, $\epsilon_r = 2.22$, $2b = 2.556\ mm$.

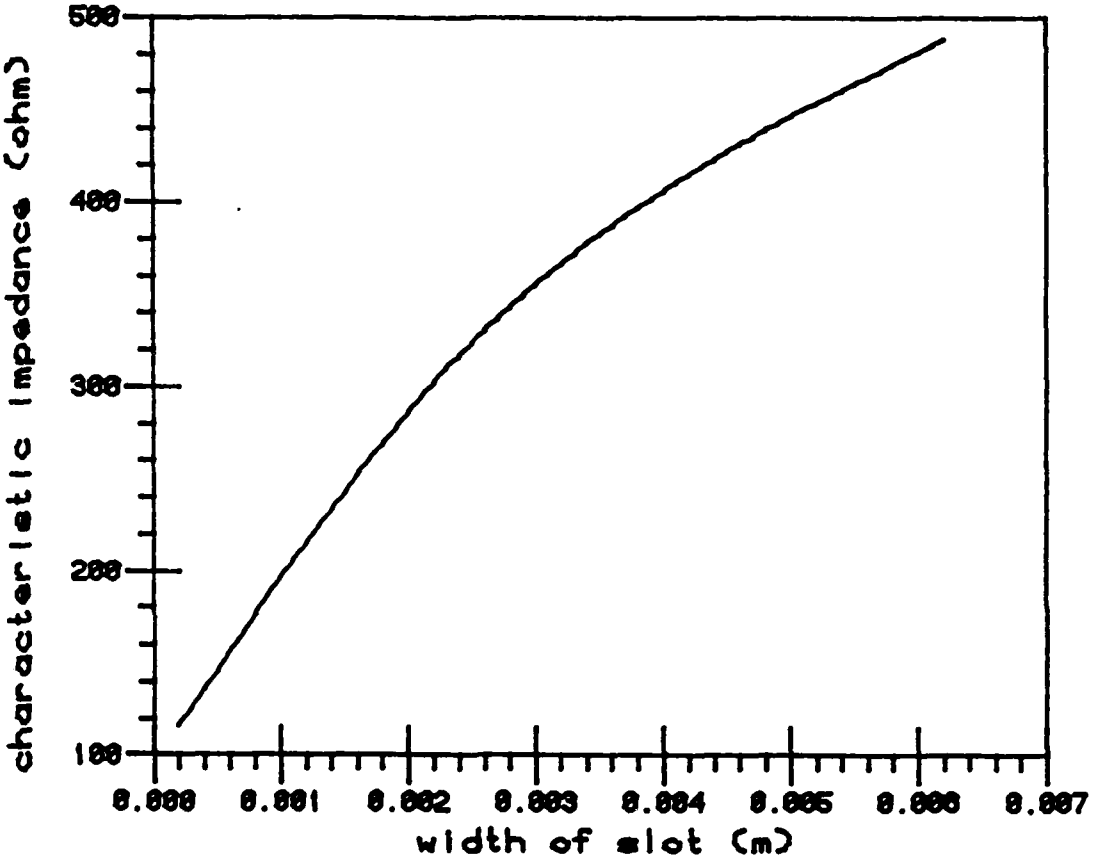

Figure 2.12. Characteristic impedance for fin-line with a WR-62 shield using a pulse approximation for E_x. $l_1 = l_2 = 7.773$ *mm*, $2d = 0.254$ *mm*, $\epsilon_r = 2.2$, $2b = 7.9$ *mm*, $f = 14$ GHz.

large k_z

$$\bar{\bar{Y}} \sim \begin{bmatrix} c_1|k_z|+c_2 & c_3 sgn(k_z) \\ c_3 sgn(k_z) & \dfrac{c_4}{|k_z|}+c_5 \end{bmatrix} \tag{2.20}$$

and for large k_x

$$\bar{\bar{Y}} \sim \begin{bmatrix} \dfrac{d_1}{|k_x|}+d_2 & d_3 sgn(k_x) \\ d_3 sgn(k_x) & d_4|k_x|+d_5 \end{bmatrix}. \tag{2.21}$$

where the c's and d's are constant coefficients.

The transverse vector mode functions are

$$\bar{e}(x,y) = \hat{x}e_x(x,y) + \hat{y}e_y(x,y) \tag{2.22a}$$

$$\bar{h}(x,y) = \hat{x}h_x(x,y) + \hat{y}h_y(x,y) \tag{2.22b}$$

These field components are plotted for a typical case in Figures 2.13 through 2.16. Notice that the fields are confined to the region around the slot. The functions represent a single propagating mode.

The solutions for the propagation constant are very stable when a relatively small number of basis functions and spectral terms are used. (i.e., a small number of spectral terms are required for convergence in the propagation constant.) However, at least an order of magnitude more spectral terms are required for convergence of the basis function coefficients. Also, an increase in the number of basis functions necessitates an increase in the number of spectral terms.

It is therefore quite difficult to find a satisfactory representation for the propagating and evanescent mode functions. The analysis of a number of fin-line problems requires the generation of a suitable set of orthogonal modes.

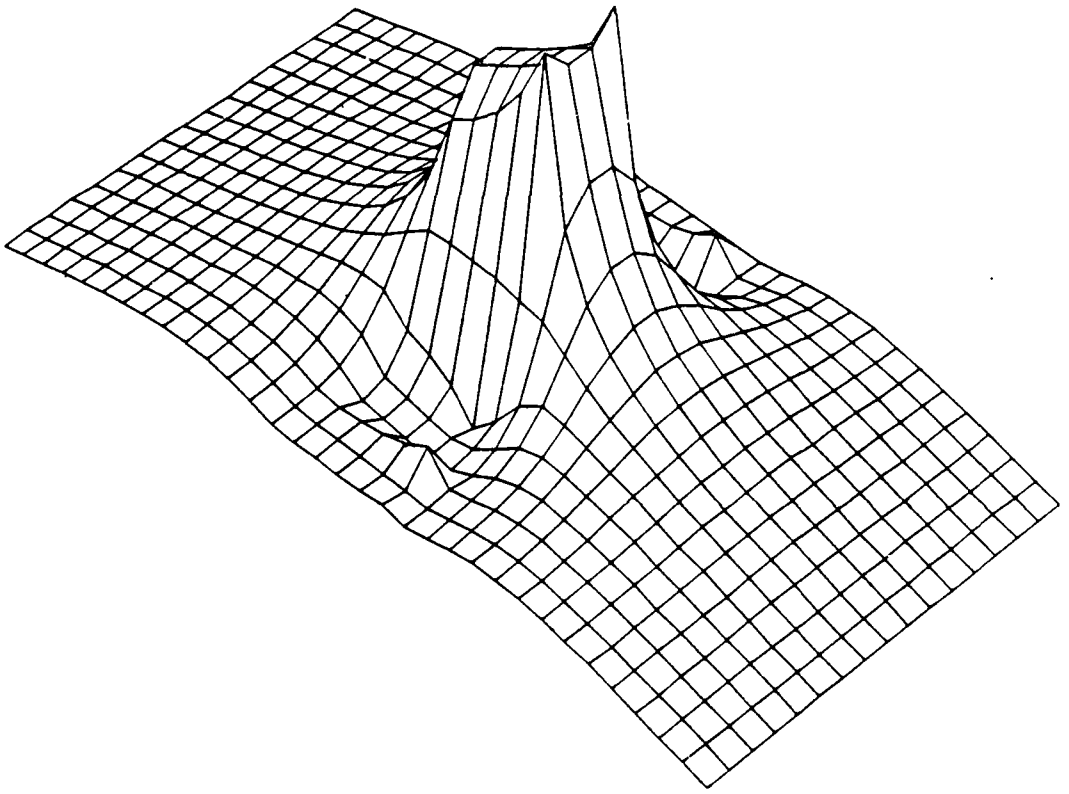

Figure 2.13. Fin-line mode function $|e_z(x,y)|$.

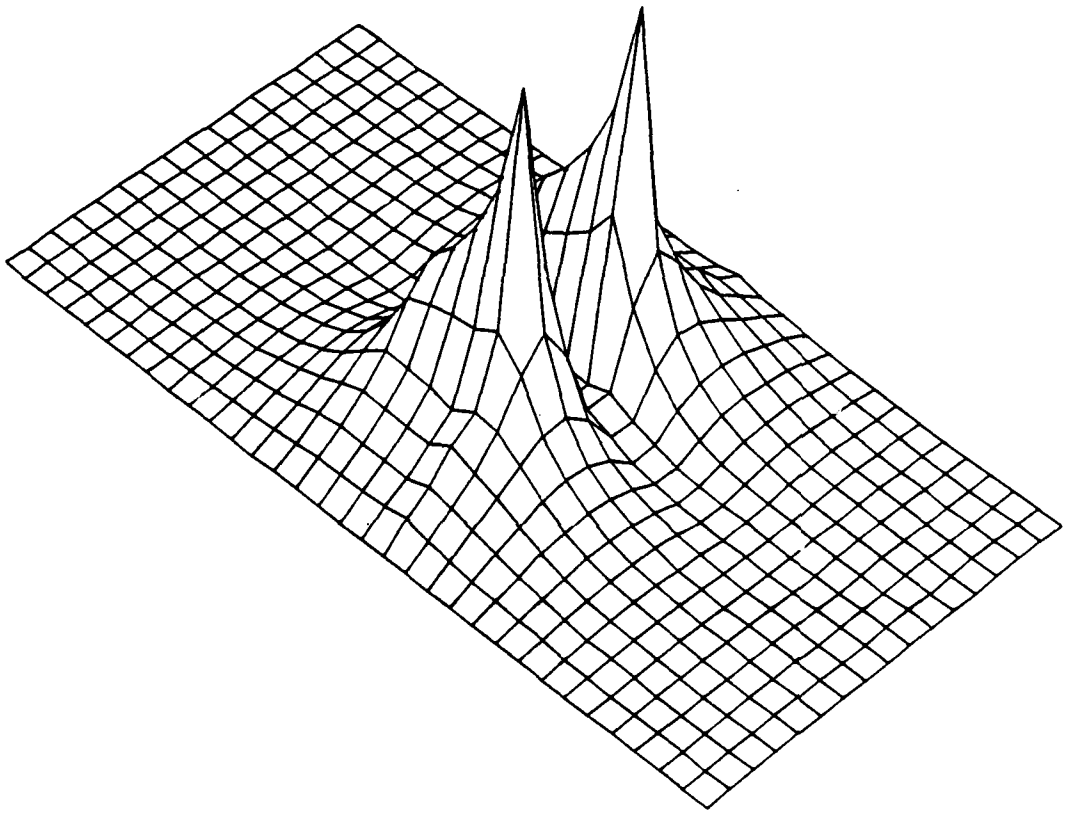

Figure 2.14. Fin-line mode function $|h_z(x,y)|$.

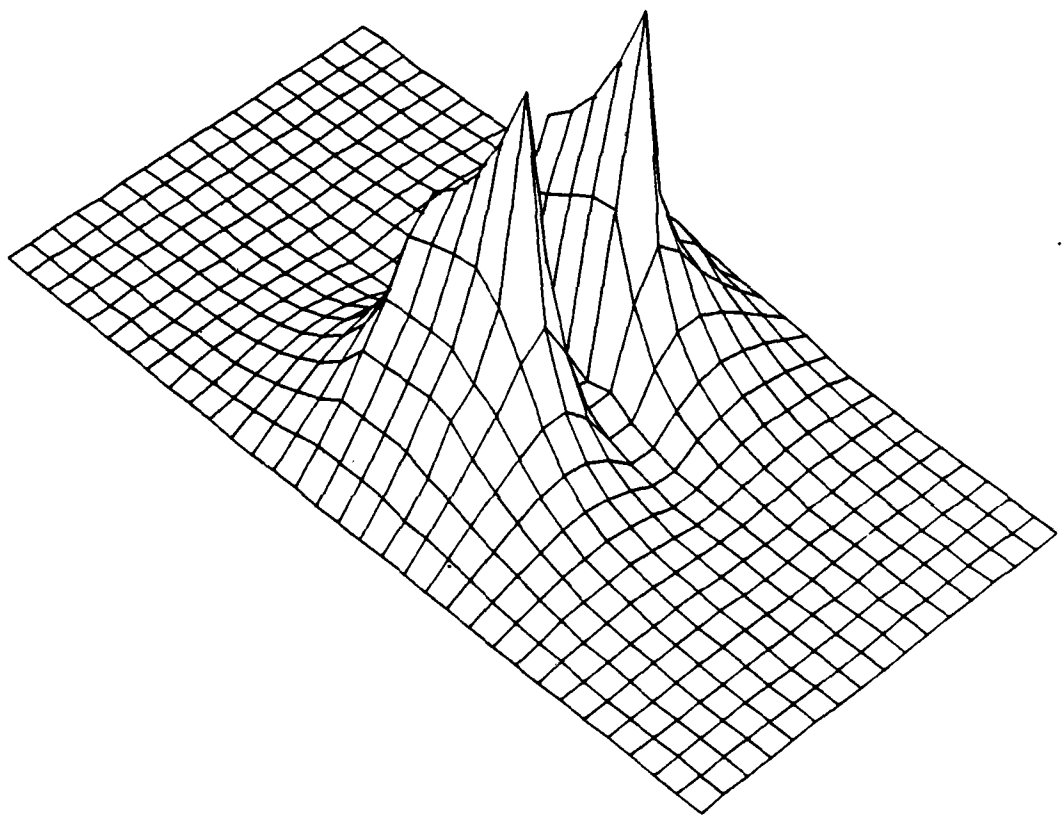

Figure 2.15. Fin-line mode function $|e_y(x,y)|$.

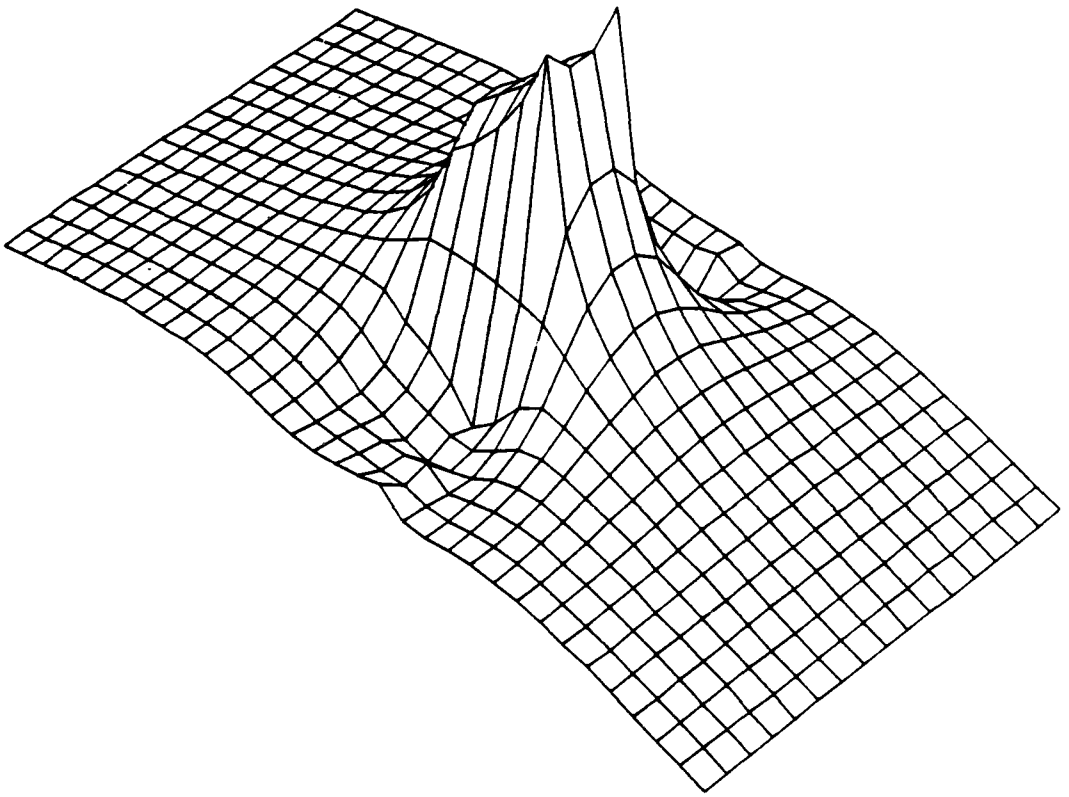

Figure 2.16. Fin-line mode function $|h_y(x,y)|$.

CHAPTER 3: MOMENT METHOD ANALYSIS OF FIN-LINE DISCONTINUITIES

3.1. The Fin-Line Discontinuity Problem

Unilateral fin-line will be considered in the discontinuity analysis. The word "discontinuity" will mean a perturbation in the slot width. A step discontinuity is shown in Fig. 3.1a. The solution of such a problem is essential for design and analysis of many millimeter-wave components.

Mode matching has been used, with some success, to analyze fin-line discontinuities [4], [7], [16], [17]. An analysis of an infinite periodic array of stubs has been published recently [18]. This approach utilizes a moment method.

This chapter considers moment method solutions which are applicable to a variety of fin-line discontinuities, including the single discontinuity of Fig. 3.1a, and the periodic array of Fig. 3.1b.

The formulation employed in this chapter reduces a three-dimensional scattering problem to a two-dimensional spectral relationship in the plane of the fin. This technique employs the known spectral Green's function, $\overline{\overline{Y}}$. A spectral domain formulation, which is an extension of the two-dimensional analysis of Chapter 2, is employed. Section 3.2 deals with the single discontinuity problem and Section 3.3 considers the infinite periodic problem. Conclusions on these techniques are drawn in Section 3.4.

3.2. Theoretical Analysis for the Single Discontinuity

The discontinuity of Fig. 3.2 will be considered for this analysis. The technique is quite general, and may be applied to other geometries. A series of discontinuities, such as Fig. 3.2, is of interest in filtering and matching applications.

A spectral relationship in the "fin-plane" may be written as a general extension of Eq. (2.6)

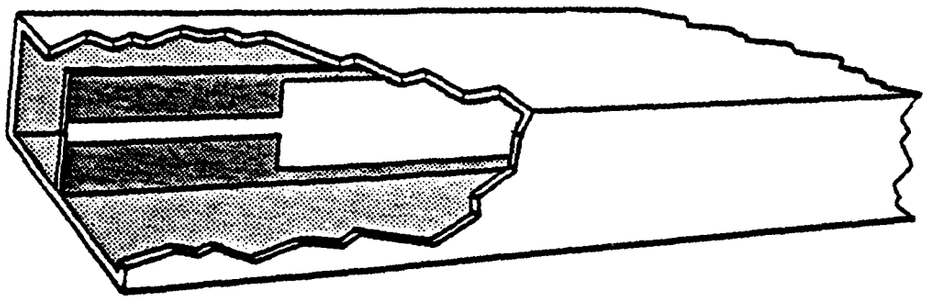

(a)

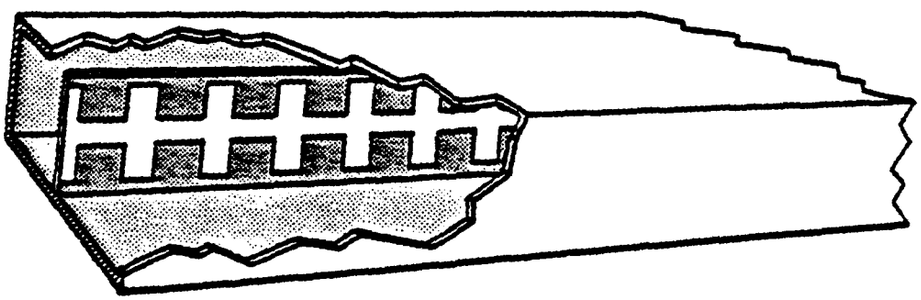

(b)

Figure 3.1. (a) Single discontinuity in fin-line, (b) array of discontinuities.

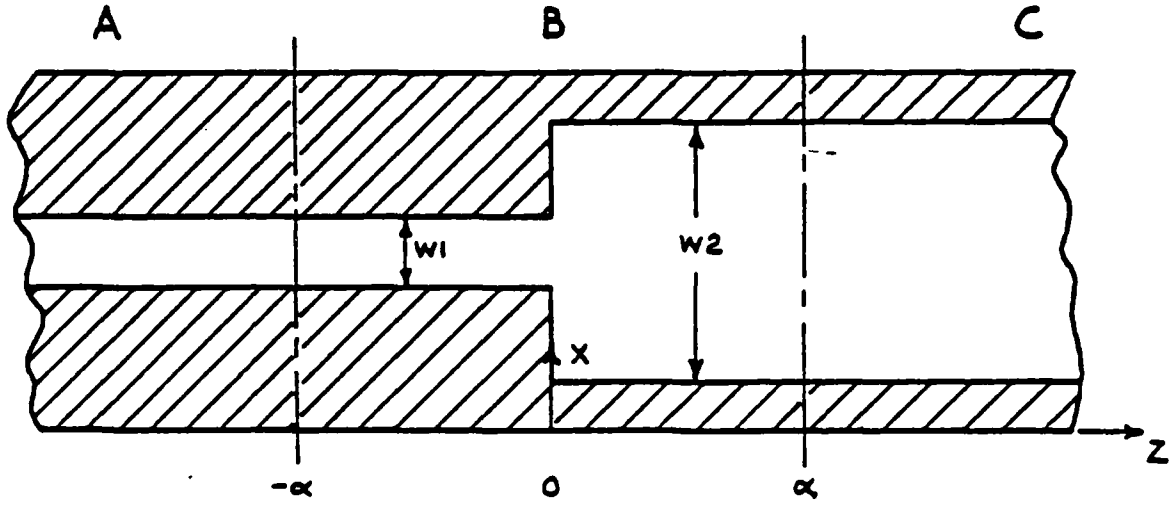

Figure 3.2. Geometry for single fin-line discontinuity.

$$\overline{\overline{Y}}(k_x,k_z)\,\tilde{\overline{E}}(k_x,k_z) = \tilde{\overline{J}}(k_x,k_z) \tag{3.1}$$

where

$$\overline{\overline{Y}}(k_x,k_z) = \begin{bmatrix} Y_{xx} & Y_{xz} \\ Y_{zx} & Y_{zz} \end{bmatrix}$$

$$\tilde{\overline{E}} = \begin{bmatrix} \tilde{E}_x \\ \tilde{E}_z \end{bmatrix}$$

$$\tilde{\overline{J}} = \begin{bmatrix} \tilde{J}_x \\ \tilde{J}_z \end{bmatrix}.$$

The spectral variable k_x is again discrete; $k_x = 2n\pi/2b$, and k_z is a continuous spectral variable for the single discontinuity problem. $\overline{\overline{Y}}$ is as for Eq. (2.7), with k_z a spectral variable rather than an eigenvalue.

A matrix equation can be obtained by applying the moment method to Eq. (3.1) with a two-dimensional inner product defined by

$$\langle \tilde{X}_i(k_x,k_z), \tilde{Y}_j(k_x,k_z) \rangle = \sum_{n=-\infty}^{\infty} \int_{-\infty}^{\infty} \tilde{X}_i^*(k_x,k_z)\,\tilde{Y}_j(k_x,k_z)\,dk_z. \tag{3.2}$$

A single propagating mode will be considered in this analysis. The desired information is the scattering parameters of the junction. Consider a three region problem, as shown in Fig. 3.2. The fields in the A- and C- regions are assumed known, except for complex constants. In Fig. 3.2, α is sufficiently large so that the evanescent modes are negligible in regions A and C. The field distributions in regions A and C are found from a uniform slot analysis and are themselves a superposition of basis functions. The slot fields in the B-region can be expressed as a superposition of suitable basis functions. We can write

$$\tilde{\overline{E}} = \tilde{\overline{E}}_A + \tilde{\overline{E}}_B + \tilde{\overline{E}}_C \tag{3.3}$$

$$\text{where } \tilde{\overline{E}}_Q = \begin{vmatrix} \tilde{E}_{Qx} \\ \tilde{E}_{Qz} \end{vmatrix} \quad Q = A, B, C$$

$$\overline{E}_Q = \overline{E}_Q^+ + \overline{E}_Q^-. \tag{3.4}$$

The (+) signifies forward traveling waves, and the (-) signifies negative traveling waves. Expressing the B-region fields in terms of a sum of basis functions,

$$E_{xB} = \sum_{i=1}^{I} a_i \, \zeta_i (x,z)$$

$$E_{zB} = \sum_{j=1}^{J} b_j \, \eta_j (x,z). \tag{3.5}$$

The fin current, $\overline{J}$, and the slot field, $\overline{E}$, are orthogonal, and by Parseval's Theorem, $\tilde{\overline{J}}$ and $\tilde{\overline{E}}$ are orthogonal. Therefore, the right-hand side of Eq. (3.1) will not contribute in the matrix equation. Of course, the matrix equation will have a right-hand side which is due to the known incident field on the junction (E_A^+). Applying a moment method to Eq. (3.1),

$$\begin{aligned} &<\tilde{\xi}_m, Y_{xx} \tilde{E}_x> + <\xi_m, Y_{xz} \tilde{E}_z> = 0 \\ &<\tilde{\psi}_n, Y_{zx} \tilde{E}_x> + <\tilde{\psi}_n, Y_{zz} \tilde{E}_z> = 0. \end{aligned} \tag{3.6}$$

This equation is of the form $Ax = b$, where x is the unknown containing the coefficients of the basis functions, and b is due to the incident field which is known.

The reflection and transmission coefficients at $z = \pm \alpha$ can be related to the unknown basis function coefficients in the B-region by integral relationships on these boundaries. Therefore, there are I + J unknowns to be solved for.

The z-dependencies for the incident (f_i), reflected (f_r), and transmitted (f_t) fields are

$$\begin{aligned} f_i(z) &= [1 - u_{-1}(z)] e^{-j\beta_1 z} \\ f_r(z) &= [1 - u_{-1}(z)] e^{-j\beta_1 z} \\ f_t(z) &= u_{-1}(z) e^{-j\beta_2 z}. \end{aligned} \tag{3.7}$$

The Fourier Transforms of these, upon application of the Weiner-Hopf technique (where a finite loss is introduced) [19], become

$$\tilde{f}_i(k_z) = \frac{1}{j(k_z - \beta_1)}$$

$$\tilde{f}_r(k_z) = \frac{1}{j(k_z - \beta_1)} \tag{3.8}$$

$$\tilde{f}_t(k_z) = \frac{-1}{j(k_z - \beta_2)}.$$

It should be noted that to reproduce the uniform solution from the formulation here, it is necessary to consider the lossless case, where impulse functions are included in the transform of Eq. (3.7).

The efficient evaluation of the integral in Eq. (3.2) is quite difficult and of prime importance. The inner product integral is of the form

$$\int_{-\infty}^{\infty} \frac{y_{ij}\, F(k_z)}{(k_z \pm \beta_n)}\, dk_z \tag{3.9}$$

where $i, j \in x, z$ and $F(k_z)$ and Y_{ij} have no real poles. The two integration contours used are shown in Fig. 3.3. Figure 3.3a is for positive traveling waves and Fig. 3.3b for negative traveling waves. The pole is located at the propagation constant for a given region. A good discussion of the contour selection for many mode problems is given in Collin and Zucker [20]. There are an infinite number along the imaginary axis due to the evanescent modes. The location of these cannot be determined simply. Therefore, the integration contour cannot be closed. It is then necessary to evaluate the principal value of the integral numerically. Davis and Rabinowitz [21] discuss methods of approximate integration over infinite intervals. Unfortunately, the techniques generally used for such integrals are not readily applied to this case. The kernel has a two-dimensional variation which makes the application of asymptotic techniques very difficult. A satisfactory truncation point for the integral must be selected to give an acceptable error. The method of foldover [22] may be applied. This technique may be summarized by

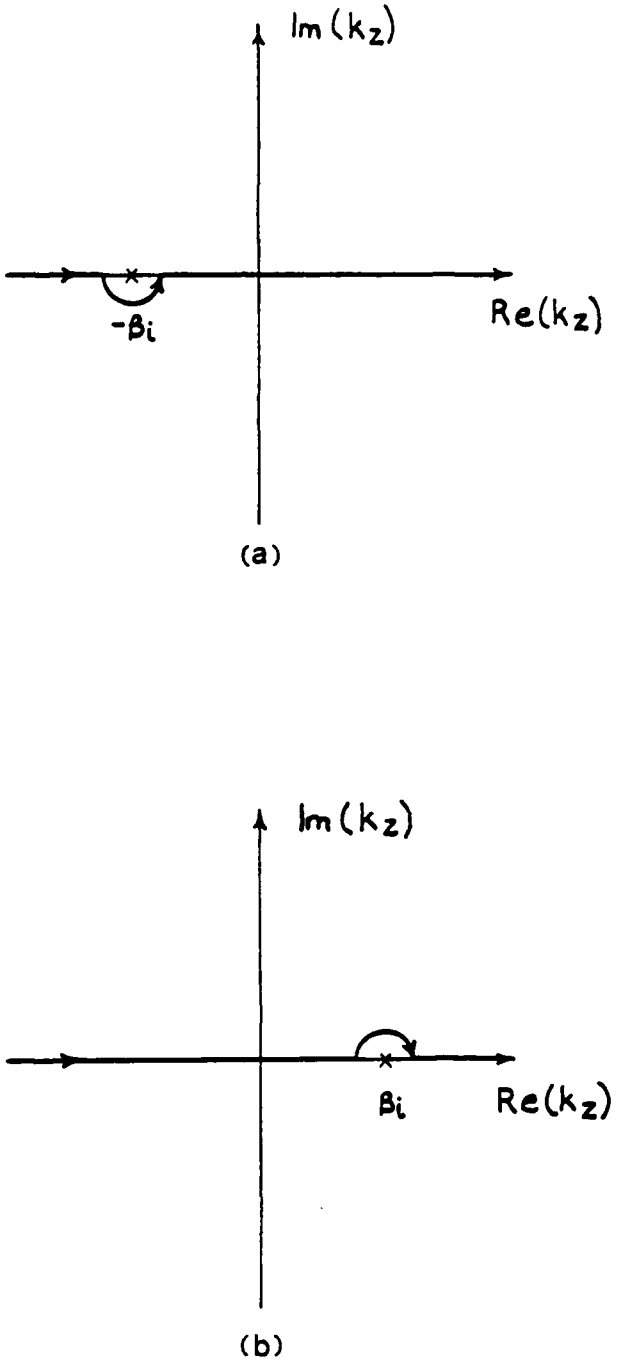

Figure 3.3. Integration contours for inner product evaluation, (a) negative travelling wave, (b) positive travelling wave.

$$\int_{-\infty}^{\infty} F_1(k_z)dk_z = \int_{-\infty}^{-\beta_1} F_1(k_z)dk_z + \int_{-\beta_1}^{\infty} F_1(k_z)dk_z + j\pi\, Res(-\beta_1).$$

$$= \int_{-\infty}^{-2\beta_1} F_1(k_z)dk_z + \int_{-\beta_1}^{0} \left| F_1(-2\beta_1 - k_z) + F_1(k_z) \right| dk_z$$

$$+ \int_{0}^{\infty} F_1(k_z)dk_z + j\pi\, Res(-\beta_1). \tag{3.10}$$

$$\int_{-\infty}^{\infty} F_2(k_z)dk_z = \int_{-\infty}^{\beta_1} F_2(k_z)dk_z + \int_{\beta_1}^{\infty} F_2(k_z)dk_z - j\pi\, Res(-\beta_1)$$

$$= \int_{-\infty}^{0} F_2(k_z)dk_z + \int_{0}^{-\beta_1} \left| F_2(k_z) + F_2(2\beta_1 - k_z) \right| dk_z$$

$$+ \int_{2\beta_1}^{\infty} F_2(k_z)dk_z - j\pi\, Res(-\beta_1). \tag{3.11}$$

The new kernel becomes bounded at the location of the singularities in the old kernel. This allows a more accurate approximation near the singularity and an increase in the speed of the computation. The kernel is oscillatory in nature, which increases the difficulty of the numerical integration.

3.3. Numerical Results for the Single Discontinuity

E_x is the dominant field component in the slot. It is, therefore, a satisfactory approximation to set $E_z = 0$. Equation (3.6) then becomes

$$< \tilde{\xi}_m, Y_{xx} \tilde{E}_x > = 0 \tag{3.12}$$

for ξ_m orthogonal to J_x.

Now consider a single pulse approximation for $E_x(x)$, so that E_x can be written as

$$E_x = (e^{-j\beta_1 z} + a_1 e^{j\beta_1 z})\, P_x(s, w_1)\,(1 - u_{-1}(z))$$
$$+ a_2 e^{-j\beta_2 z}\, P_x(s, w_2) u_{-1}(z) \tag{3.13}$$

where β_1 and β_2 are the propagation constants for the dominant mode for z < 0 and z > 0, respectively. The testing functions used are

$$\xi_1(x, z) = P_x(s, w_1)\, P_z(\frac{-\alpha}{2}, \alpha)\, e^{j\beta_1 z}$$
$$\xi_2(x, z) = P_x(s, w_2)\, P_z(\frac{-\alpha}{2}, \alpha)\, e^{j\beta_2 z}. \tag{3.14}$$

The integral in Eq. (3.2) has been evaluated numerically using both the IMSL routine DCADRE and the trapezoidal scheme. A more efficient computer program can be written using the trapezoidal rule. Integral limits of $\pm 15\,\beta_1$ with nineteen spectral terms in the k_x summation prove to be adequate for convergence. A trapezoidal integration with 700 points is suitable. The foldover method is used in the integral evaluation.

The scattering parameters of the junction computed by this procedure are not stable with respect to variations in the pulse length α. While somewhat reasonable results can be achieved for certain cases, the approach of testing a semi-infinite unknown with a finite pulse does not give reliable results.

If loss is introduced into the basis functions of Eq. (3.13) and Galerkin's method is used in Eq. (3.12), the poles move off the real k_z axis. The unknowns are tested over the entire semi-infinite region. The scattering parameters vary significantly as a function of the loss coefficient.

3.4. Theoretical Analysis for an Infinite Periodic Array of Discontinuities

A unit cell in an infinite array is shown in Fig. 3.4. The spectral relationship of Eq. (3.1) can be applied to this geometry. However, now k_z takes on discrete values.

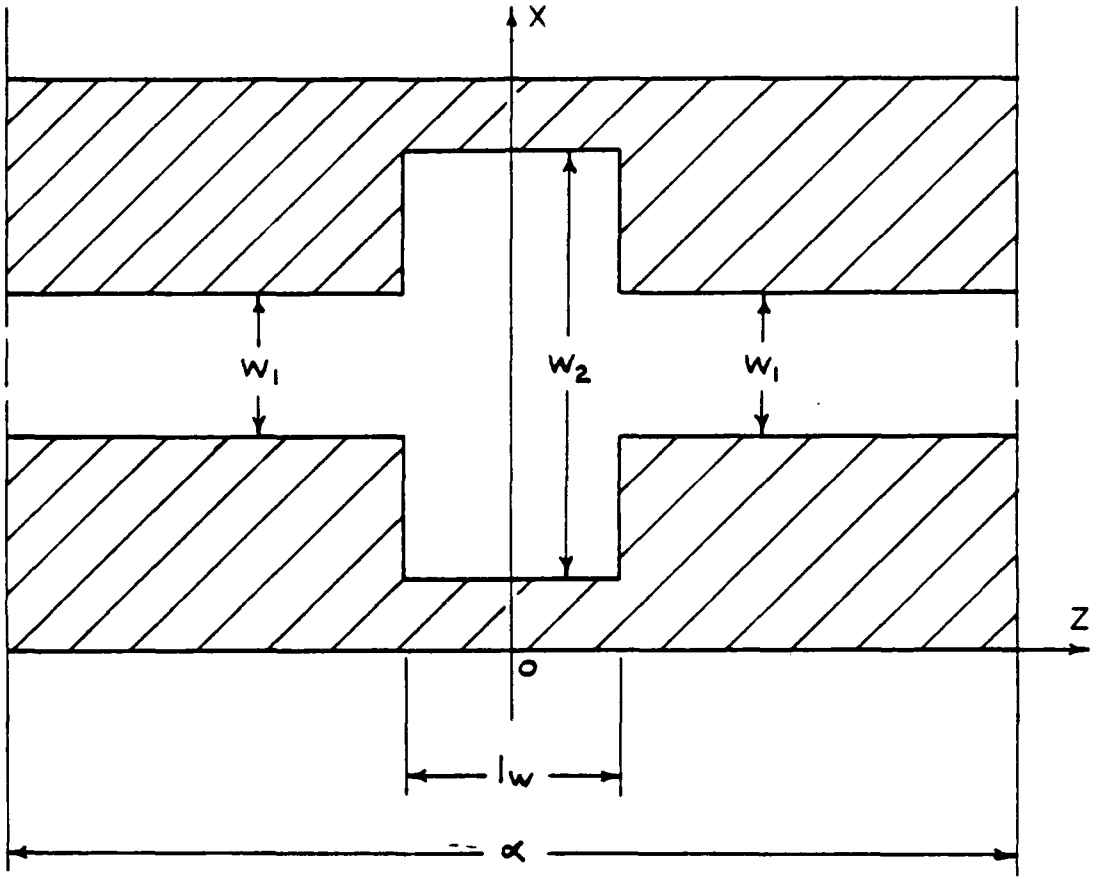

Figure 3.4. Unit cell in an infinite periodic array of discontinuities.

A discussion of periodic structures is given in Collin and Zucker [20]. Floquet's Theorem may be used to relate the field quantities at $z = -\alpha$ and $z = \alpha$. The fields may be expanded in a Fourier series in the z-direction. For the E-field,

$$E_q(x,y,z) = \sum_{n=-\infty}^{\infty} E_{qn}(x,y)e^{-j\beta_n z}$$

$$E_{qn}(x,y) = \frac{1}{\alpha}\int_{-\alpha/2}^{\alpha/2} E_q(x,y,z)\, e^{j\beta_n z}\, dz \tag{3.15}$$

where $q \in \{x,z\}$

$$\beta_n = \beta_o + \frac{2n\pi}{\alpha}.$$

In the application of Eq. (3.1) to this geometry, field quantities in the plane of the fin ($y = l_1 + 2d$) are considered. E_x and E_z in this plane can be expanded in terms of appropriate functions, and a homogeneous equation of the form Ax = 0 can then be obtained by using Galerkin's method.

Consider a representation for E_x and E_z given by

$$E_x(x,z) = \sum_{i=1}^{I} a_i\, \zeta_i(x,z)$$

$$E_z(x,z) = \sum_{j=1}^{J} b_j\, \eta_j(x,z). \tag{3.16}$$

The weighting for the discrete spectral terms is given by

$$\tilde{\zeta}_i(k_x,\beta_n) = \frac{1}{2b\alpha}\int_{-\alpha/2}^{\alpha/2}\int_{0}^{2b} \zeta_i(x,z)\; e^{j(k_x x + \beta_n z)}\, dx\, dz$$

$$\tilde{\eta}_j(k_x,\beta_n) = \frac{1}{2b\alpha}\int_{-\alpha/2}^{\alpha/2}\int_{0}^{2b} \eta_j(x,z)\; e^{j(k_x x + \beta_n z)}\, dx\, dz. \tag{3.17}$$

The homogeneous equation becomes

$$\sum_n <\tilde{\zeta}_p, Y_{xx} \sum_{i=1}^{I} a_i \tilde{\zeta}_i> + \sum_n <\tilde{\zeta}_p, Y_{xz} \sum_{j=1}^{J} b_j \tilde{\eta}_j> = 0. \qquad p = 1,\ldots,I$$

$$\sum_n <\tilde{\eta}_q, Y_{zx} \sum_{i=1}^{I} a_i \tilde{\zeta}_i> + \sum_n <\tilde{\eta}_q, Y_{zz} \sum_{j=1}^{J} b_j \tilde{\eta}_j> = 0. \qquad q = 1,\ldots,J \tag{3.18}$$

The solution of det(A) = 0, where A is the operator matrix in Eq. (3.18), gives the solution for β_n

Consider the $(k_o\alpha\,,\,\beta\alpha)$ diagram shown in Fig. 3.5. Several coupled modes are shown in this diagram. Stopbands occur when $\beta\alpha$ equals an integral multiple of π. When $\beta\alpha = \pi$, coupling occurs between the n = 0 Floquet mode and the n = -1 mode. That is, there is coupling between a forward traveling wave and a negative traveling wave. Note that the example in Fig. 3.5 is for a TEM wave in a periodically loaded media which has no low-frequency cutoff.

The analysis outlined here is implemented numerically in the next section. This gives an approximation to the $(k_o\alpha\,,\,\beta\alpha)$ curve over a particular range. The range of interest here is $0 \leqslant \beta\alpha \leqslant \pi$.

3.5. Numerical Results for an Infinite Periodic Array of Discontinuities

The $(k_o\alpha,\beta\alpha)$ diagram for an infinite periodic array of discontinuities, as shown in Fig. 3.1(b), is determined in this section. The basis functions used to approximate the fields in Eq. (3.16) are

$$\zeta_1(x,z) = P_x(s,w_1)\,P_z(0,\alpha)$$

$$\zeta_2(x,z) = P_x(s,w_1)\left[P_z(0,\alpha) - P_z(0,L_w)\right] sgn(z)$$

$$\eta_1(x,z) = 2\frac{(x-s)}{w}\sqrt{1-\left|2\frac{(x-s)}{w}\right|^2}. \tag{3.19}$$

The computed results for a portion of the $(k_o\alpha\,,\,\beta\alpha)$ diagram are shown in Fig. 3.6 together with the fin-line dimensions for this example. The approximation used for the slot fields results in some spuri-

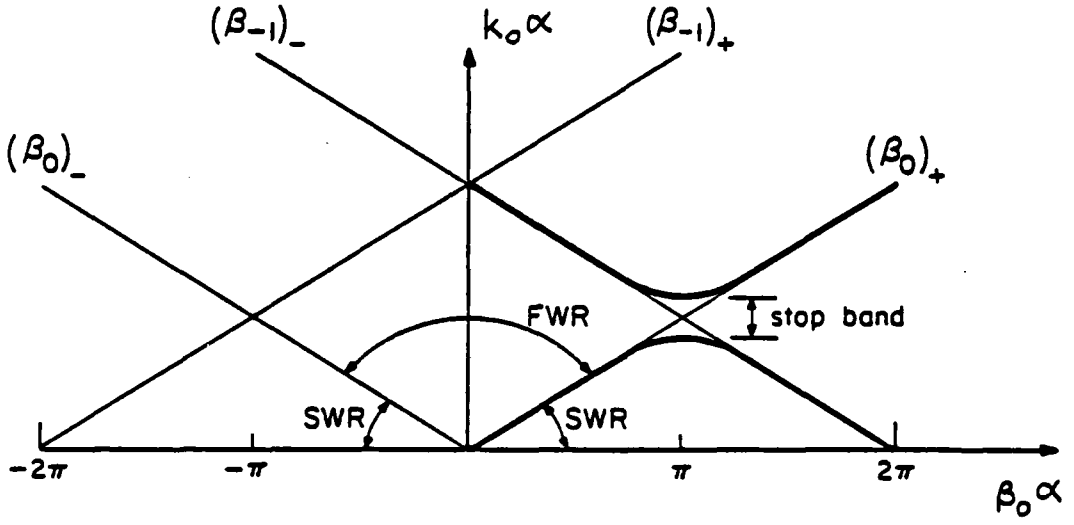

Figure 3.5. $(k_o\alpha\ ,\ \beta\alpha)$ diagram for a TEM wave in a periodically loaded media.

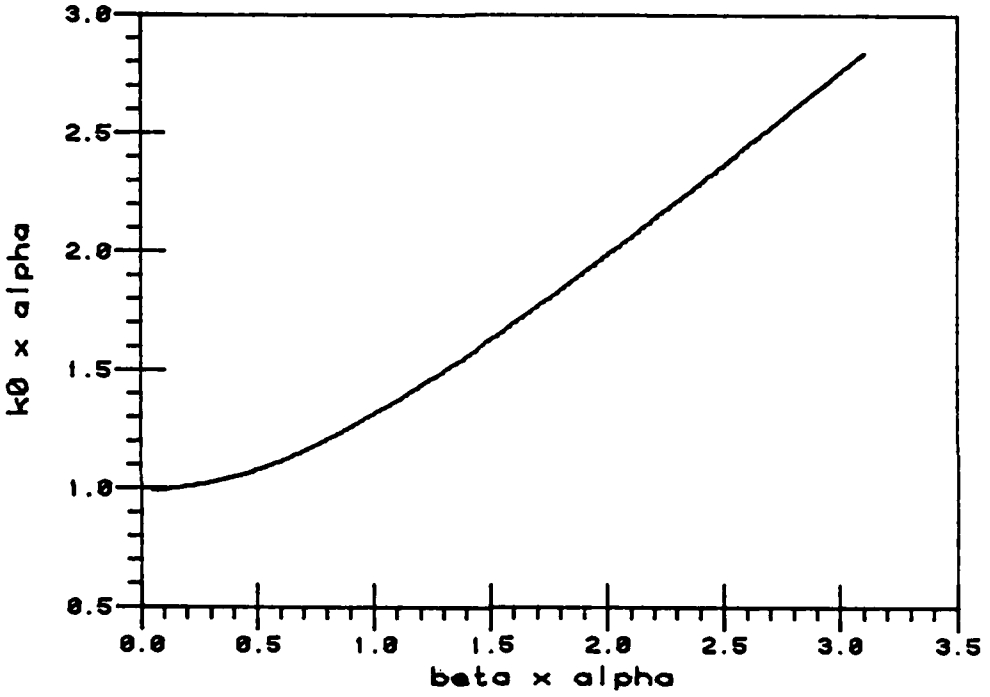

Figure 3.6. Computed ($k_0\alpha$, $\beta\alpha$) diagram for fin-line in a WR-28 shield. $l_1 = l_2 = 3.429$ *mm*, $2d = 0.254$ *mm*, $\epsilon_r = 2.22$, $2b = 2.556$ *mm*, $w_1 = 0.2$ *mm*, $w_2 = 2.0$ *mm*, $l_w = 0.2$ *mm*, $\alpha = 4.4$ *mm*.

ous solutions near $\beta d = \pi$ and poor sensitivity to discontinuity variations.

3.6. Concluding Remarks

This chapter used a two-dimensional spectral relationship in the fin plane, between the slot fields and the fin currents. The moment method was then used to solve for the slot fields. Both the problem of a single step discontinuity and an infinite periodic array of discontinuities were studied. In the case of the single discontinuity, efficient evaluation of the inner product integrals is important to minimize computation time.

CHAPTER 4: ITERATIVE AND VARIATIONAL SOLUTIONS FOR FIN-LINE DISCONTINUITIES

4.1. Introduction

This chapter considers various iterative solutions for the fin-line discontinuity problem. The discontinuity considered in this chapter is that of Section 3.2 which is shown again in Fig. 4.1. The emphasis of this chapter will be on two iterative procedures which are applied to a suitable formulation.

Solution of electromagnetic problems using iterative techniques is advantageous when there are a large number of unknowns. In fact, when there are a very large number of unknowns, it is the only way to find a solution. If the number of unknowns is such that the matrix can be inverted on the computer being used, the moment method may be preferable.

The discontinuity problem is formulated using unknowns in the junction plane, in Section 4.2. The solution procedure using a conjugate gradient iterative scheme is outlined in Section 4.3. Numerical results for the conjugate gradient method are given in Section 4.4. Solution for the junction plane unknowns using the generalized variational procedure is outlined in Section 4.5, and numerical results are given in Section 4.6. Conclusions are drawn in Section 4.7.

4.2. Formulation using Unknowns in the Junction Plane

A waveguide junction problem can be formulated using the mode functions either side of the discontinuity [23]. Consider the general junction of Fig. 4.2. The transverse field can be expressed in terms of the mode functions in guides A and B. Consider I modes

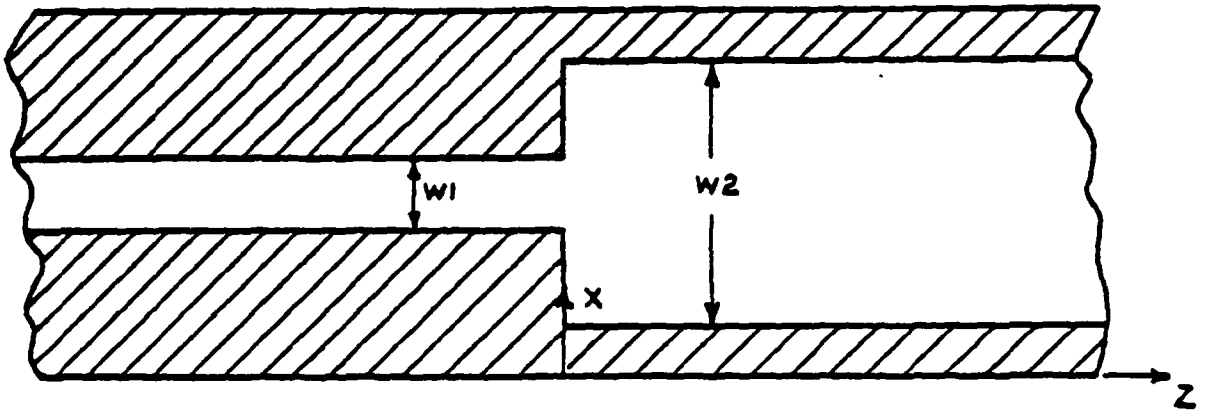

Figure 4.1. Single step discontinuity in unilateral fin-line.

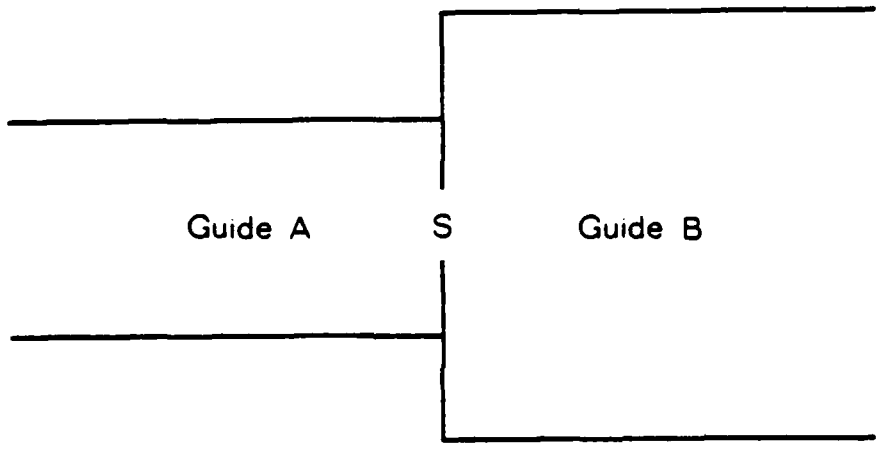

Figure 4.2. General junction between two waveguides.

$$\overline{E}_t = \begin{cases} \bar{e}_{ai}\, e^{-\gamma_{ai} z} + \sum_{i=1}^{I} a_i \bar{e}_{ai}\, e^{\gamma_{ai} z} & z < 0 \\ \sum_{i=1}^{I} b_i\, \bar{h}_{bi}\, e^{-\gamma_{bi} z} & z > 0 \end{cases} \tag{4.1a}$$

$$\overline{H}_t = \begin{cases} \bar{h}_{ai}\, e^{-\gamma_{ai} z} - \sum_{i=1}^{I} a_i \bar{h}_{ai}\, e^{\gamma_{ai} z} & z < 0 \\ \sum_{i=1}^{I} b_i \bar{h}_{bi}\, e^{-\gamma_{bi} z} & z > 0 \end{cases} \tag{4.1b}$$

Rather than pursuing the regular mode-matching formulation, consider an alternate approach as follows. Figure 4.3 shows an equivalent representation for the junction, employing equivalent magnetic currents over the apertures. The total transverse field for the equivalent problem is

$$\overline{E}_t = \begin{cases} \bar{e}_{ai}\, e^{-\gamma_{ai} z} - \bar{e}_{ai}\, e^{\gamma_{ai} z} + \sum_{i=1}^{I} d_i\, \bar{e}_{ai}\, e^{\gamma_{ai} z} & z < 0 \\ \sum_{i=1}^{I} b_i\, \bar{e}_{bi}\, e^{-\gamma_{bi} z} & z > 0 \end{cases} \tag{4.2a}$$

$$\overline{H}_t = \begin{cases} \bar{h}_{ai}\, e^{-\gamma_{ai} z} + \bar{h}_{ai}\, e^{\gamma_{ai} z} - \sum_{i=1}^{I} d_i\, \bar{h}_{ai}\, e^{\gamma_{ai} z} & z < 0 \\ \sum_{i=1}^{I} b_i \bar{h}_{bi}\, e^{-\gamma_{bi} z} & z > 0 \end{cases} \tag{4.2b}$$

The fields produced in guide A by K are $\overline{E}_a(\overline{K})$, $\overline{H}_a(\overline{K})$, and in guide B by $-\overline{K}$ are $\overline{E}_b(-\overline{K})$, $\overline{H}_b(-\overline{K})$. For continuity of $\overline{E}_t$,

$$\overline{K} = \hat{z}\times\overline{E}_a(\overline{K})|_{z=0} = \sum_{i=1}^{I} d_i\, \hat{z}\times\bar{e}_{ai}$$

$$\overline{K} = \hat{z}\times\overline{E}_b(-\overline{K})|_{z=0} = \sum_{i=1}^{I} b_i\, \hat{z}\times\bar{e}_{bi}. \tag{4.3}$$

Continuity of $\overline{H}_t$ requires

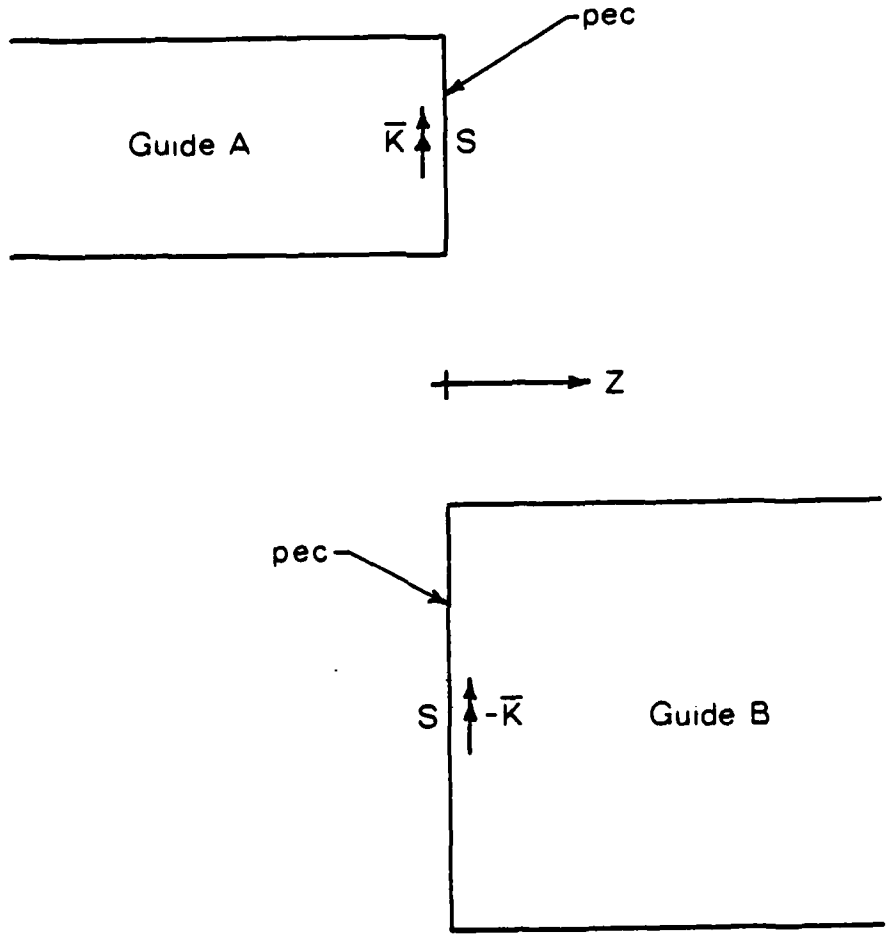

Figure 4.3. Equivalent waveguide junction problem.

$$2\,\bar{h}_{a1} = \sum_{i=1}^{I} d_i \bar{h}_{ai} + \sum_{i=1}^{I} b_i \bar{h}_{bi}. \tag{4.4}$$

The solution for the unknown quantity, $\overline{K}$, could be obtained via several numerical approaches. The solution for k via certain iterative techniques is of interest in this chapter.

Taking inner products of Eq. (4.3), and using the orthogonality of Eq. (2.18) with normalized mode functions,

$$\begin{aligned}
\iint_s \bar{h}_{ak} \cdot \overline{K}\, ds &= \sum_{i=1}^{I} d_i \iint_s \bar{h}_{ak} \cdot \hat{z}\times\bar{e}_{ai}\, ds \\
&= d_k \\
\iint_s \bar{h}_{bk} \cdot \overline{K}\, ds &= \sum_{i=1}^{I} b_i \iint_s \bar{h}_{bk} \cdot \hat{z}\times\bar{e}_{bi}\, ds \\
&= b_k .
\end{aligned} \tag{4.5}$$

Substitution for the d's and b's in Eq. (4.4) results in an integral equation which may be used to solve for the unknown operative magnetic current $\overline{K}$.

$$\begin{aligned}
2\,\bar{h}_{ai}(x,y) = &\sum_{i=1}^{I} \bar{h}_{ai}(x,y) \iint_s \bar{h}_{ai}(x',y') \cdot \overline{K}(x',y')\,dx'dy' \\
&+ \sum_{i=1}^{I} \bar{h}_{bi}(x,y) \iint_s \bar{h}_{bi}(x',y') \cdot \overline{K}(x',y')\,dx'dy'.
\end{aligned} \tag{4.6}$$

This equation may be interpreted in terms of the Green's function for each guide as follows. The dyadic Green's function can be found simply from the mode functions using a procedure outlined in Collin and Zucker [24]. Equation (4.6) can be written as

$$2\bar{h}_1 = \int_s \int [\bar{\bar{G}}_a + \bar{\bar{G}}_b][\bar{K}]\, ds'$$

where

$$\bar{h}_i = \begin{vmatrix} h_{aix}(x,y) \\ h_{aiy}(x,y) \end{vmatrix}$$

$$\bar{K} = \begin{vmatrix} K_x(x,y) \\ K_y(x,y) \end{vmatrix}$$

$$\bar{\bar{G}}_q = \begin{vmatrix} \sum_{i=1}^{I} h_{aix}(x,y)h_{qix}(x',y') & \sum_{i=1}^{I} h_{qix}(x,y)h_{qiy}(x',y') \\ \sum_{i=1}^{I} h_{aiy}(x,y)h_{qix}(x',y') & \sum_{i=1}^{I} h_{qiy}(x,y)h_{qiy}(x',y') \end{vmatrix} \tag{4.7}$$

$q \in \{a,b\}$.

For the fin-line discontinuity of Fig. 4.1, the aperture is the cross-section of the shielding enclosure. The number of modes, I, in each guide will be small due to the difficulty of finding a large number of orthogonal modes.

Following the solution for $\bar{K}$, the mode coefficients can be found using Eq. (4.5). The scattering parameters can then be determined from these mode coefficients following a re-normalization for unit power. Assuming that the modes have been normalized for $\int_s \int \bar{e}_n \times \bar{h}_n\, ds = 1$, the scattering parameters for the single propagating mode are given by

$$S_{n1} = \int_s \int \bar{h}_{q1} \cdot \bar{K}\, ds \; \frac{\left| \int_s \int \bar{e}_{ai} \times \bar{h}_{ai}\, ds \right|^{1/2}}{\left| \int_s \int \bar{e}_{q1} \times \bar{h}_{q1}\, ds \right|^{1/2}}. \tag{4.8}$$

$q \in \{a,b\}$

$n \in \{1,2\}$.

4.3. Conjugate Gradient Solution for Unknowns in the Junction Plane

The conjugate gradient method [25]-[28] has been in existence for some time. However, it is only recently that it has been applied to the solution of electromagnetic problems [27]. The method was developed by Hestenes and Stiefel [25].

For n unknowns, the method will converge in n steps, if no rounding-off errors occur. The method is quite simple. At each step, the estimate is an improvement over the previous step, and the process can be restarted at any step using the last value as the new initial estimate.

Consider the linear equation $L\ f\ = g$, where L is a general non-singular matrix. $L^A L$ is a positive definite operator, but is in general non-symmetric. The system $L\ f\ = g$ is equivalent to

$$L^A L f\ = L^A g. \tag{4.9}$$

Another equivalent equation, which results in a symmetric, but not a positive definite operator, is $L^T L f\ = L^T g$. The conjugate gradient technique may be applied to Eq. (4.9). The iterative scheme is

$$\begin{aligned}
r_o &= g - L f_o \\
p_o &= L^A r_o \\
a_i &= \frac{\| L^A r_i \|^2}{\| L p_i \|^2} \\
f_{i+1} &= f_i + a_i p_i \\
r_{i+1} &= r_i - a_i L p_i \\
b_i &= \frac{\| L^A r_{i+1} \|^2}{\| L^A r_i \|^2} \\
p_{i+1} &= L^A r_{i+1} + b_i p_i .
\end{aligned} \tag{4.10}$$

The inner products in this scheme are defined such that $\| f \|^2 = < f , f >$ and $< f , L f > = < L^A f , f >$.

An estimate f_o of the unknown f is used to generate the residual r_o and the direction p_o. In each cycle, following the determination of the estimate f_i, the residual r_i and the direction p_i, the next estimates for $f_{i+1}, r_{i+1}, p_{i+1}$ are computed. The residuals $r_o, r_1, \cdots$ are mutually orthogonal, and the direction vectors $p_o, p_1, \cdots$ are mutually conjugate, therefore

$$\begin{aligned} &< r_i, r_j > = 0 \qquad i \neq j \\ &< p_i, Lp_j > = 0. \end{aligned} \tag{4.11}$$

Each estimate f_{i+1} will be closer to the solution than f_i. The norm-squared of the residual can be used as a measure of the error

$$err_i = \| r_i \|^2. \tag{4.12}$$

However, this is not alway reliable, as $\| r_i \|^2$ may not decrease at each step.

Consider now the fin-line discontinuity problem of interest, which is shown in Fig. 4.1. This problem was formulated in Section 4.2. The conjugate gradient method can be applied to Eq. (4.6) to solve for $\overline{K}(x,y)$. The unknowns are K_x and K_y over a grid of points in the (x,y) plane at z = 0. An (m,n) set of grid points represents $2mn$ unknowns. A reasonable approximation for the unknown requires a large number of unknowns.

The inner product for this problem is given by

$$< x, y > = \int_s \int x^* y \, dx dy. \tag{4.13}$$

4.4. Numerical Results for the Conjugate Gradient Solution in the Junction Plane

The mode functions are found using the procedure outlined in Chapter 2, resulting in $\bar{e}_n(k_x, y)$, $\bar{h}_n(k_x, y)$. For convenience, many of the processes in the iterative routine of Eq. (4.10) are carried out in the spectral domain. The Fast Fourier Transform is utilized throughout for transformations in the x-direction. Although there are $2mn$ total unknowns (for an (m,n) array of points),

(m,n) arrays may be used throughout the computer program.

As indicated in Chapter 2, it is difficult to obtain a large set of orthogonal mode functions for use in the Green's function. This necessitates computation with as few as three modes.

The limiting case of a uniform slot is a good example to consider first. A relative error will be used as a figure of merit, where the residual is normalized to the incident field.

$$rel.\ err_i = \frac{\|r_i\|^2}{\|e_{a1}\|^2} \tag{4.14}$$

Figure 4.4 shows the results at each iteration using a poor initial estimate of $k_x = k_y = 0 + j0$. Notice the rapid convergence to the solution. This data is for $m=17, n=33$ $w_1 = w_2 = 1mm$ and three modes. There are therefore 1122 unknowns. Using a DEC VAX 11/780 computer, ten iterations using this array size require approximately sixteen seconds cpu time. This time can be reduced somewhat by using a radix-two FFT and zero padding.

Applying the same procedure to the case of differing slot widths on either side of the junction does not yield such satisfactory results. Figure 4.5 shows the results for $m=17, n=33$, $w_1 = 1mm, w_2 = 2mm$ and three modes. s_{11} goes to one because the iterative scheme finds a solution which corresponds to a higher-order mode, and is orthogonal to the Green's function modes in one region. The conclusion is that with the small number of modes which can realistically be found and the large number of degrees of freedom in the unknown, this approach will not yield satisfactory results. It is necessary to have the number of unknowns similar to the number of modes in the Green's function. Similar results are obtained when the number of grid points is quadrupled.

4.5. Solution in the Junction Plane Using the Generalized Variational Technique

The approach presented here also considers unknowns in the (x,y) plane of the junction. Again consider Eq. (4.6), which is of the form $Lf = g$, where L is an integral operator, f is the unknown, and g is the known incident field.

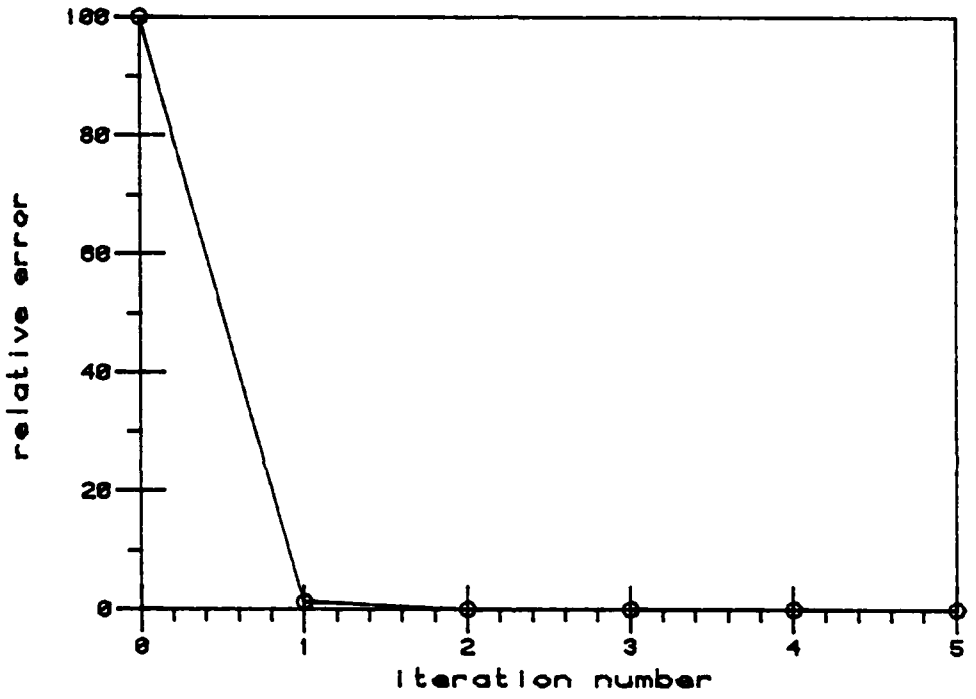

Figure 4.4. Relative error for the conjugate gradient solution of a uniform fin-line with a WR-28 shield. $l_1 = l_2 = 3.429$ *mm*, $2d = 0.254$ *mm*, $\epsilon_r = 2.22$, $2b = 2.556$ *mm*, $w_1 = w_2 = 1$ *mm*, $f = 30$ GHz, $m = 17$, $n = 33$. The resultant scattering parameters are: $S_{11} = 1.192 \times 10^{-5} + j\ 1.0486 \times 10^{-6}$, $S_{21} = 1.000 + j\ 1.049 \times 10^{-6}$.

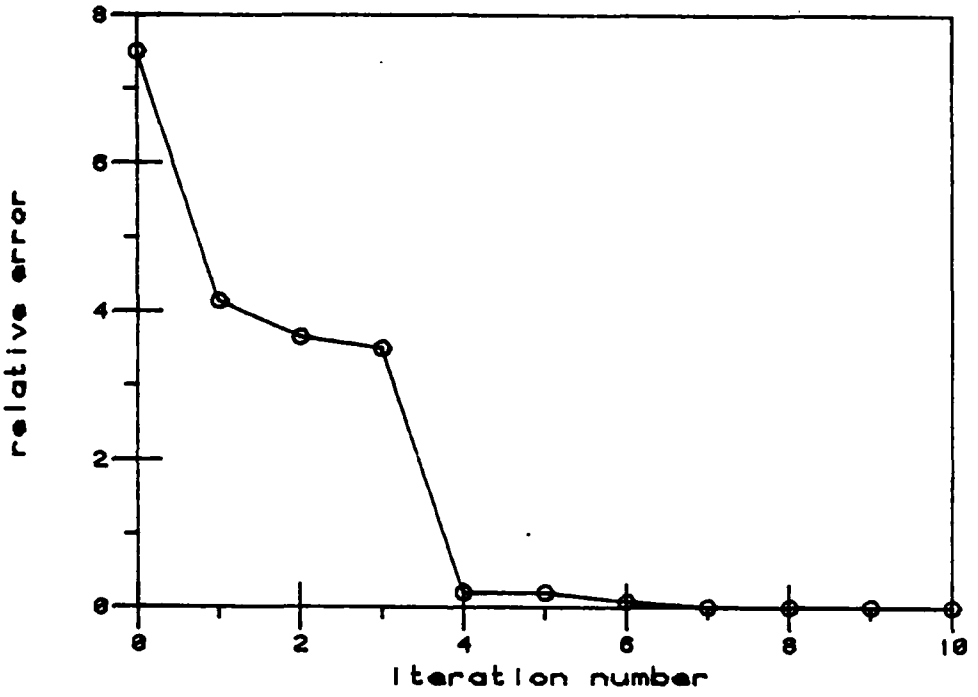

Figure 4.5. Relative error for the conjugate gradient solution of a discontinuity in fin-line with a WR-28 shield. $l_1 = l_2 = 3.429$ *mm*, $2d = 0.254$ *mm*, $\epsilon_r = 2.22$, $2b = 2.556$ *mm*, $w_1 = 1$ *mm*, $w_2 = 2$ *mm*, $f = 30$ GHz, $m = 17$, $n = 33$. The resultant scattering parameters are: $S_{11} = 1.000 + j\,6.487 \times 10^{-3}$ $S_{21} = -1.904 \times 10^{-3} + j\,1.636 \times 10^{-2}$.

The unknown quantity x may be expressed as a superposition of characteristic functions which are to be determined. f can be expressed as

$$f = \sum_{n=0}^{N} c_n f_n . \tag{4.15}$$

The f_n are L-orthogonal, and satisfy

$$< f_n, L f_m > = \eta_n \delta_{nm} \tag{4.16}$$

where δ_{mm} is the Kronecker delta function. A suitable set of characteristic functions can be generated by

$$f_n = \frac{u_n}{\| u_n \|^2} + f_{n-1} \tag{4.17}$$

where u_n is an auxiliary function which satisfies the orthogonality property

$$< u_n, u_m > = \xi_n \ \delta_{nm} . \tag{4.18}$$

The auxiliary function can be found by

$$u_n = u_{n-1} - \zeta_{n-1} L x_{n-1} \tag{4.19}$$

$$\textit{where} \quad \zeta_{n-1} = \frac{1}{\eta_{n-1}} .$$

From Eqs. (4.15) and (4.16),

$$c_n = \frac{1}{\eta_{ln}} \ . f_n, k > . \tag{4.20}$$

The generation routine can be summarized as

$$f_o = \frac{u_o}{\|u_o\|^2}$$

$$\eta_n = \langle f_n, L f_n \rangle$$

$$c_n = \frac{\langle f_n, g \rangle}{\eta_n}$$

$$u_{n+1} = u_n - \frac{1}{\eta_n} L f_n$$

$$f_{n+1} = \frac{u_{n+1}}{\|u_{n+1}\|^2} + f_n. \tag{4.21}$$

The generalized variational technique may also be applied to the equation $L^A L f = L^A g$, where now the generation routine becomes

$$f_o = \frac{u_o}{\|u_o\|^2}$$

$$\eta_n = \langle f_n, L^A L f_n \rangle$$

$$c_n = \frac{\langle f_n, L^A g \rangle}{\eta_n}$$

$$u_{n+1} = u_n - \frac{1}{\eta_n} L^A L f_n$$

$$f_{n+1} = \frac{u_{n+1}}{\|u_{n+1}\|^2} + f_n. \tag{4.22}$$

These routines can be used to solve for the unknown magnetic current in the junction plane of the fin-line discontinuity. A good choice for f_o is $\hat{z} \times \bar{e}_{a1}$, where $\bar{e}_{a1}$ is the incident transverse E-field mode function, with a possible alternative being $\hat{z} \times (\bar{e}_{a1} + \bar{e}_{b1})$. The coefficients c_n, and successive characteristic functions f_n are generated by Eq. (4.21) or Eq. (4.22).

4.6. Numerical Results for the Generalized Variational Solution of the Fin-Line Discontinuity Problem

The results in this section are generated using three modes in the Green's function. Two basis functions for E_x and E_z are used to generate the modes. Referring to Eqs. (2.8) and (2.9), these functions are for $p = 0, 1$ and $q = 2, 4$. It is important to verify that the numerical results satisfy the

following relationship for the single propagating mode.

$$|S_{11}|^2 + |S_{21}|^2 = 1. \qquad 4.23$$

Referring to Eq. (4.21) and Eq. (4.22), u_0 is chosen as $\hat{z}\times\bar{e}_{a1}$. Two different unilateral fin-line geometries are considered. There is a shortage of data from other authors for comparative purposes.

Figures 4.6-4.9 show the computed scattering parameters for a step discontinuity in fin-line with a WR-28 shield. The equation $Lf = g$ is used with one and two characteristic functions. A monotonically convergent solution as a function of the number of characteristic functions is not guaranteed. A comparison with the mode-matching data in [17] is given. However, it appears that Eq. (4.23) is not satisfied well in [17], so definite conclusions cannot be drawn regarding the accuracy. A comparison between the equations $Lf = g$ with one and two characteristic functions and the equation $L^A Lf = L^A g$ with two characteristic functions is given in Figs. 4.10-4.13.

The scattering parameters for a step discontinuity in fin-line with a WR-62 shield are shown in Figs. 4.14-4.17. The equation $Lf = g$ is used here. Equivalent circuits for this problem using S_{11} have been generated by ElHennawy and Schunemann [16] using a mode matching technique. A comparison with these results is given. An indication of the modal solution accuracy and the satisfaction of Eq. (4.23) cannot be determined from the work of ElHennawy and Schunemann [4], [16]. An approximate convergence criterion for the maximum number of characteristic functions p with q modes in the Green's function q is $p \leq q-1$.

4.7. Concluding Remarks

This chapter considered two procedures for evaluating unknowns in the cross-sectional plane of the fin-line discontinuity. The scattering parameters, or equivalent circuit for the discontinuity, may be found from these unknowns.

The conjugate gradient method was considered first. It did not give satisfactory results for the discontinuity problem. This was because the number of degrees of freedom in the unknown was

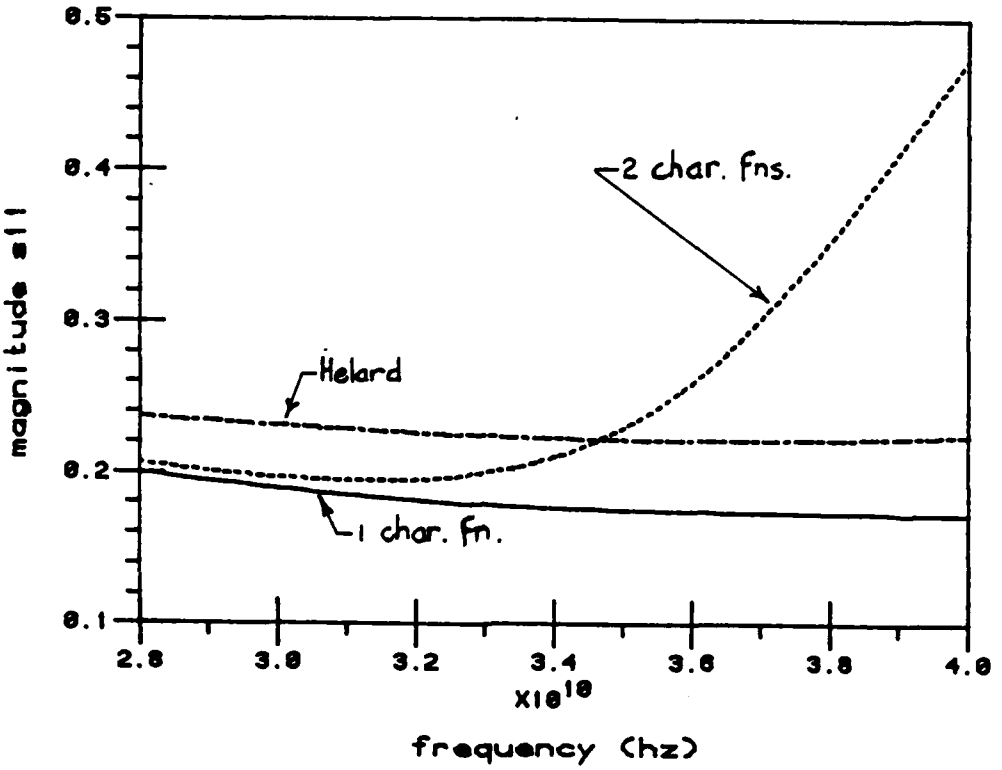

Figure 4.6. $|S_{11}|$ for a discontinuity in fin-line with a WR-28 shield. $l_1 = l_2 = 3.429$ *mm*, $2d = 0.254$ *mm*, $\epsilon_r = 2.22$, $2b = 2.556$ *mm*, $w_1 = 1$ *mm*, $w_2 = 2$ *mm*, $m = 17$, $n = 33$.

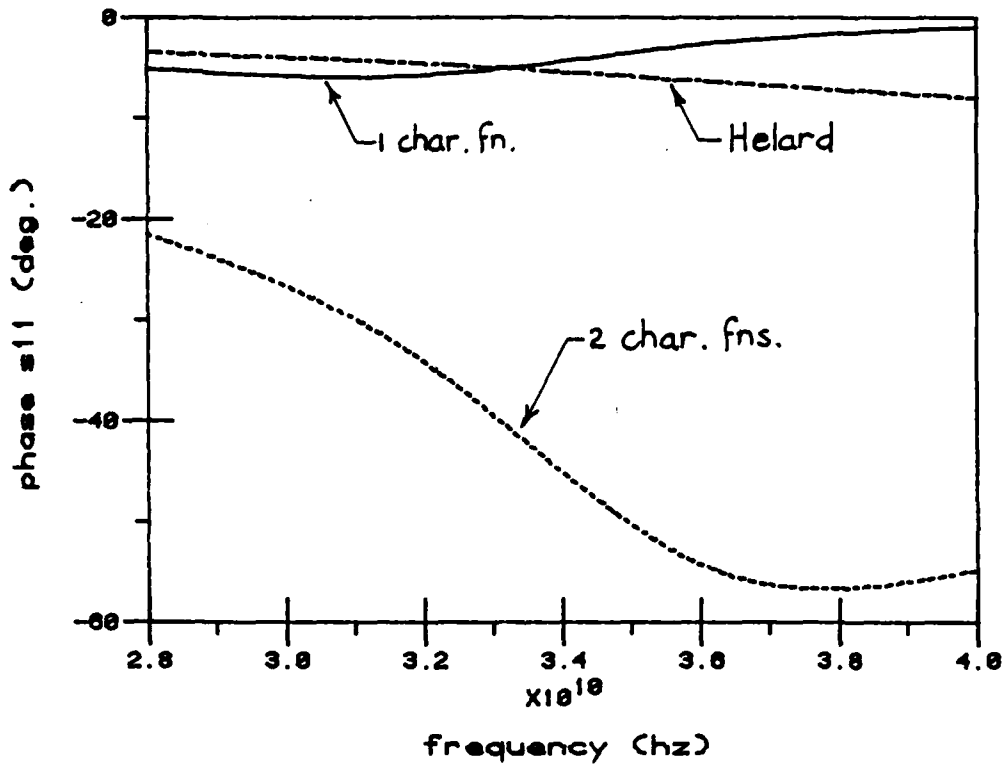

Figure 4.7. Phase (S_{11}) for a discontinuity in fin-line with a WR-28 shield. $l_1 = l_2 = 3.429$ *mm*, $2d = 0.254$ *mm*, $\epsilon_r = 2.22$, $2b = 2.556$ *mm*, $w_1 = 1$ *mm*, $w_2 = 2$ *mm*, $m = 17$, $n = 33$.

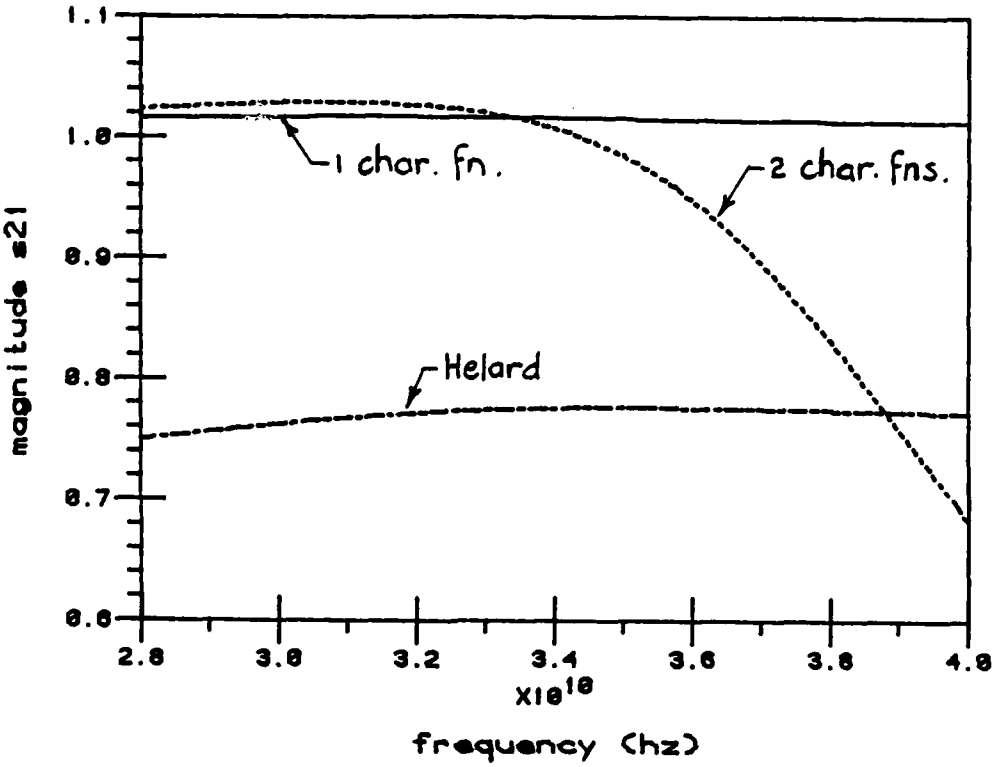

Figure 4.8. $|S_{21}|$ for a discontinuity in fin-line with a WR-28 shield. $l_1 = l_2 = 3.429$ *mm*, $2d = 0.254$ *mm*, $\epsilon_r = 2.22$, $2b = 2.556$ *mm*, $w_1 = 1$ *mm*, $w_2 = 2$ *mm*, $m = 17$, $n = 33$.

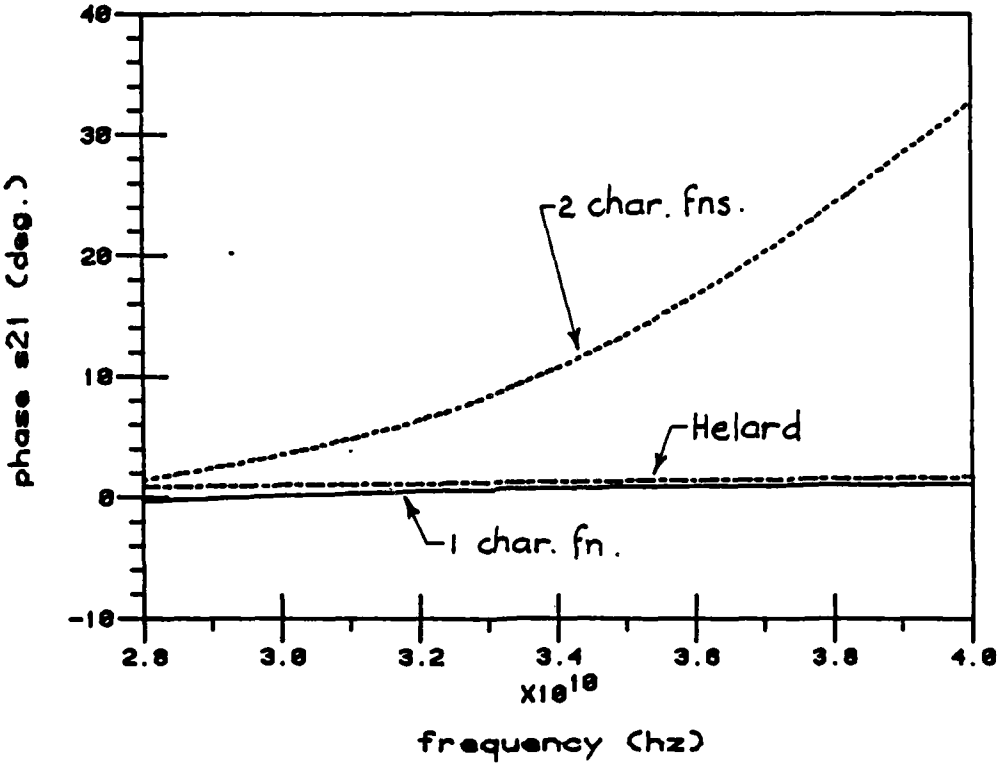

Figure 4.9. Phase(S_{21}) for a discontinuity in fin-line with a WR-28 shield. $l_1 = l_2 = 3.429$ *mm*, $2d = 0.254$ *mm*, $\epsilon_r = 2.22$, $2b = 2.556$ *mm*, $w_1 = 1$ *mm*, $w_2 = 2$ *mm*, $m = 17$, $n = 33$.

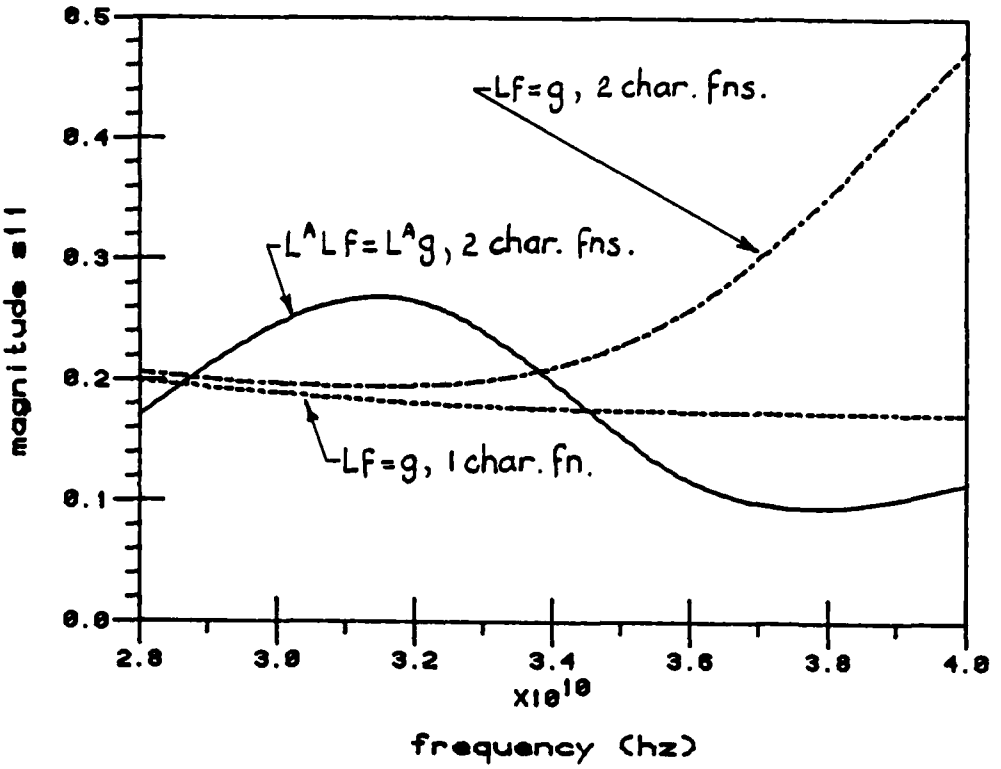

Figure 4.10. $|S_{11}|$ for a discontinuity in fin-line with a WR-28 shield. $l_1 = l_2 = 3.429$ *mm*, $2d = 0.254$ *mm*, $\epsilon_r = 2.22$, $2b = 2.556$ *mm*, $w_1 = 1$ *mm*, $w_2 = 2$ *mm*, $m = 17$, $n = 33$.

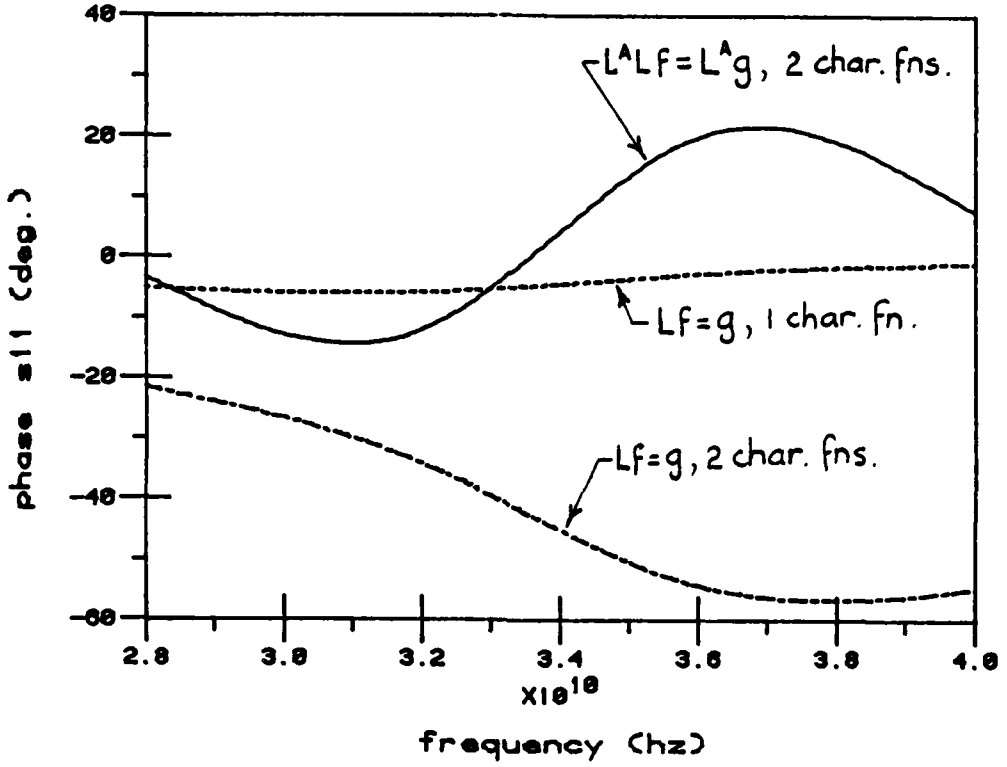

Figure 4.11. Phase (S_{11}) for a discontinuity in fin-line with a WR-28 shield. $l_1 = l_2 = 3.429mm$, $2d = 0.254\ mm$, $\epsilon_r = 2.22$, $2b = 2.556\ mm$, $w_1 = 1\ mm$, $w_2 = 2\ mm$, $m = 17$, $n = 33$.

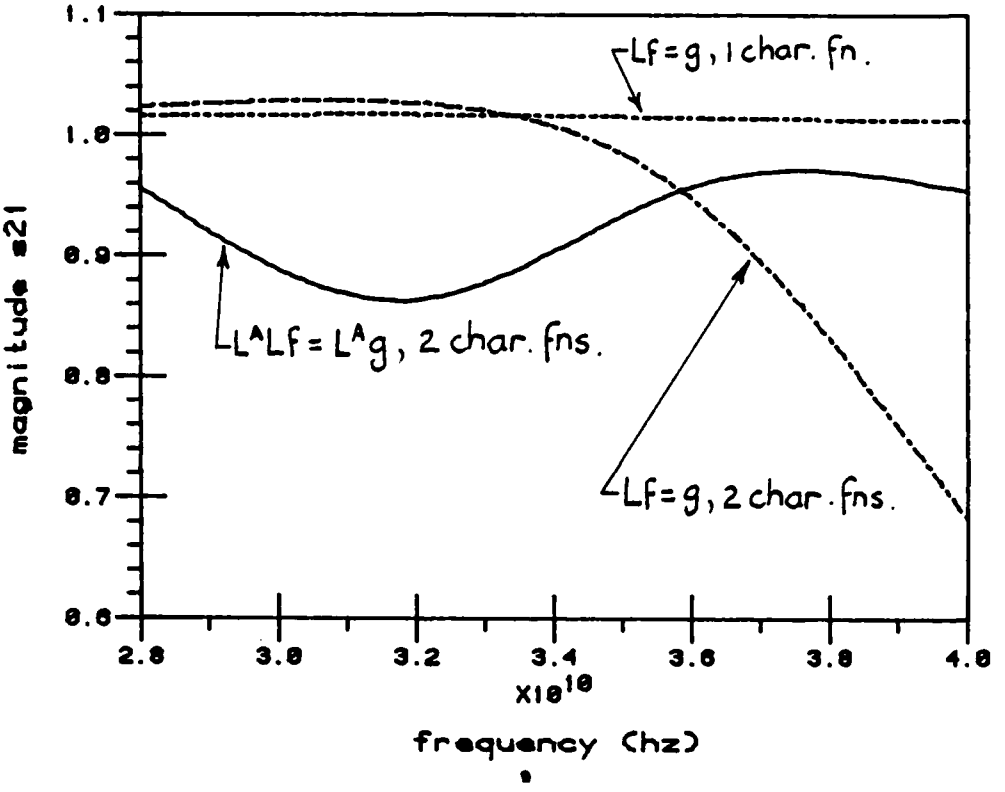

Figure 4.12. $|S_{21}|$ for a discontinuity in fin-line with a WR-28 shield. $l_1 = l_2 = 3.429$ *mm*, $2d = 0.254$ *mm*, $\epsilon_r = 2.22$, $2b = 2.556$ *mm*, $w_1 = 1$ *mm*, $w_2 = 2$ *mm*, $m = 17$, $n = 33$.

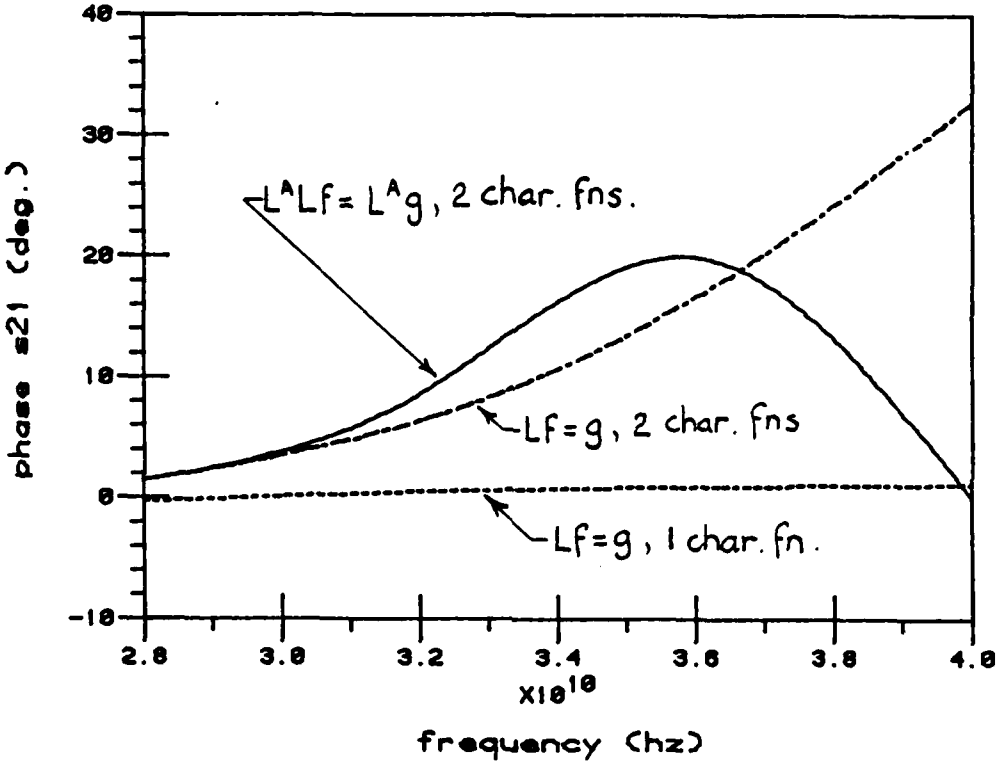

Figure 4.13. Phase(S_{21}) for a discontinuity in fin-line with a WR-28 shield. $l_1 = l_2 = 3.429$ *mm*, $2d = 0.254$ *mm*, $\epsilon_r = 2.22$, $2b = 2.556$ *mm*, $w_1 = 1$ *mm*, $w_2 = 2$ *mm*, $m = 17$, $n = 33$.

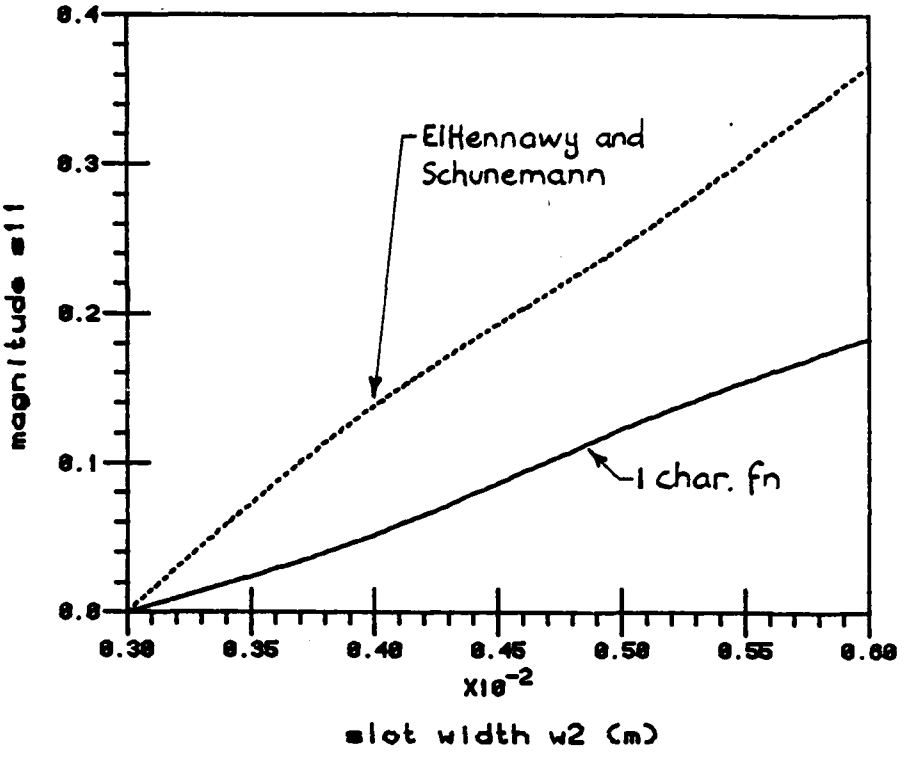

Figure 4.14. $|S_{11}|$ for a discontinuity in fin-line with a WR-62 shield. $l_1 = l_2 = 7.773$ *mm*, $2d = 0.254$ *mm*, $\epsilon_r = 2.2$, $2b = 3.95$ *mm*, $w_1 = 3$ *mm*, $m = 17$, $n = 33$.

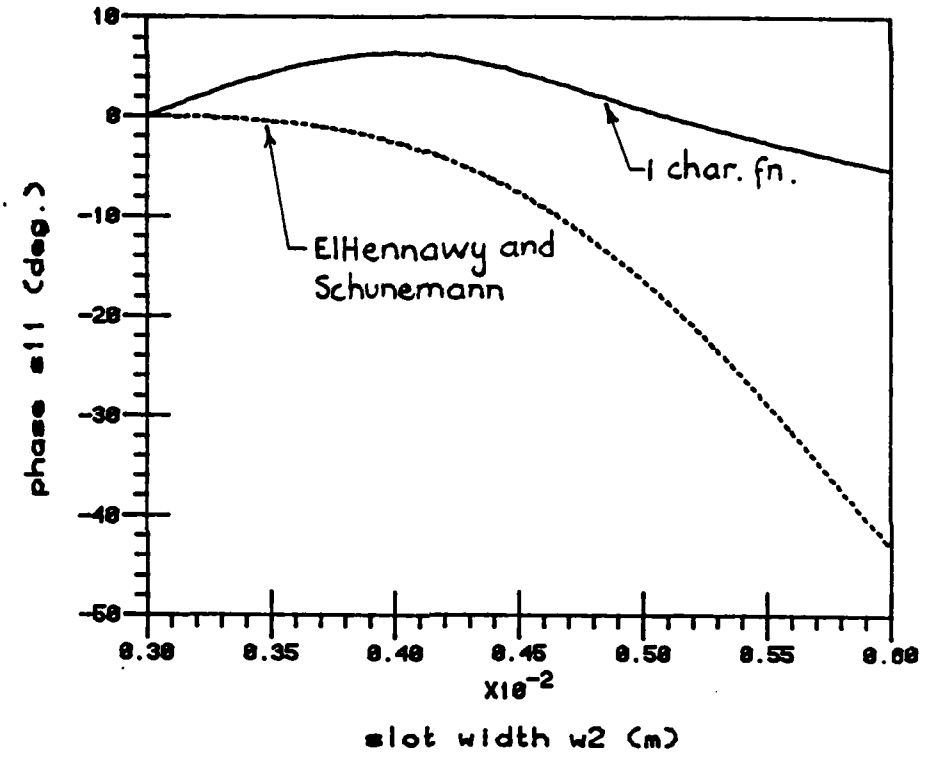

Figure 4.15. Phase (S_{11}) for a discontinuity in fin-line with a WR-62 shield. $l_1 = l_2 = 7.773$ *mm*, $2d = 0.254$ *mm*, $\epsilon_r = 2.2$, $2b = 3.95$ *mm*, $w_1 = 3$ *mm*, $m = 17$, $n = 33$.

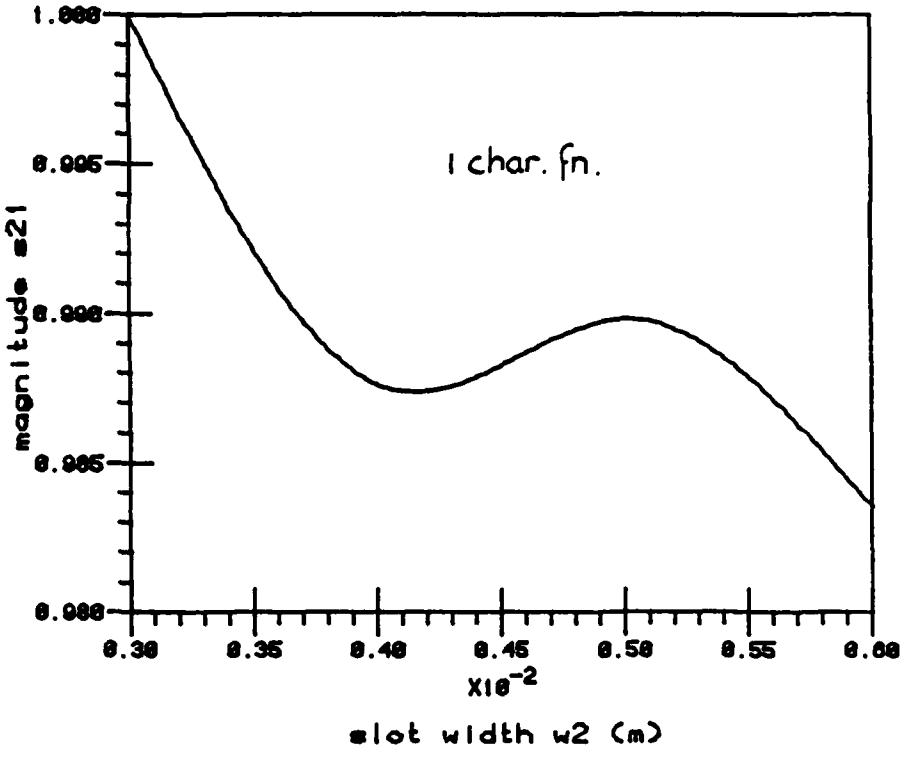

Figure 4.16. $|S_{21}|$ for a discontinuity in fin-line with a WR-62 shield. $l_1 = l_2 = 7.773$ *mm*, $2d = 0.254$ *mm*, $\epsilon_r = 2.2$, $2b = 3.95$ *mm*, $w_1 = 3$ *mm*, $m = 17$, $\tilde{n} = 33$.

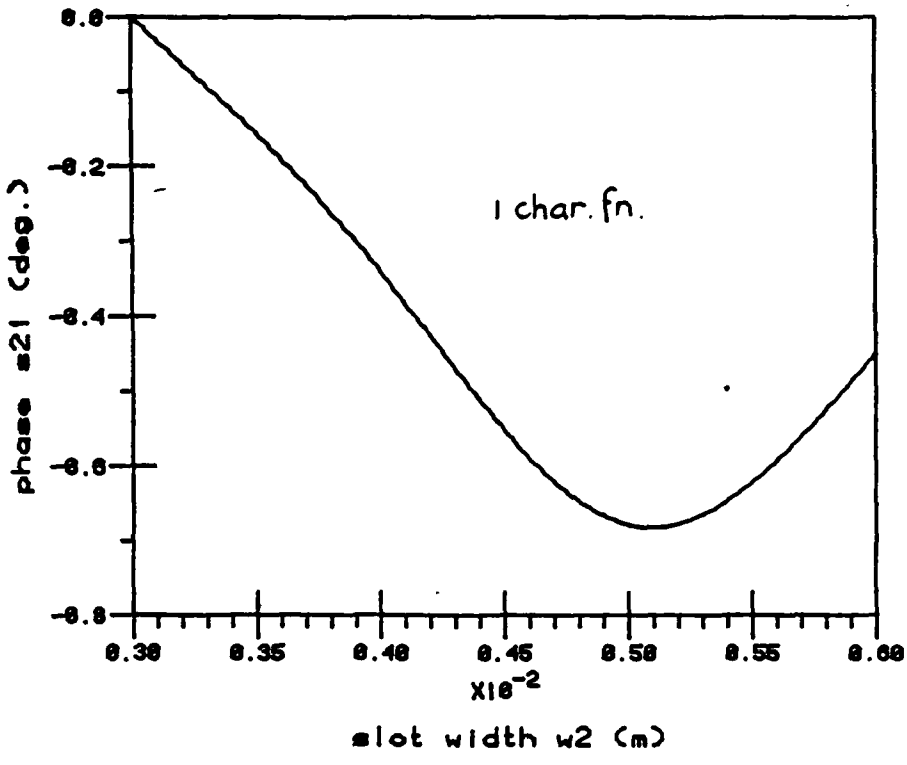

Figure 4.17. Phase(S_{21}) for a discontinuity in fin-line with a WR-62 shield. $l_1 = l_2 = 7.773$ *mm*, $2d = 0.254$ *mm*, $\epsilon_r = 2.2$, $2b = 3.95$ *mm*, $w_1 = 3$ *mm*, $m = 17$, $n = 33$.

much greater than terms, or modes, in the Green's function. It is not realistic to find a large number of modes for the Green's function. The uniform guide solution was reconstructed very efficiently.

The other approach outlined was the generalized variational technique, which involved representing the junction plane magnetic current in terms of characteristic functions. The routine for generating these functions and determining their coefficients was outlined. The results using this approach were satisfactory.

The difficulty of finding an accurate large set of mode functions is a limitation of the approaches covered in this chapter. For this reason, it is advantageous to look at alternate formulations which do not require the generation of these mode functions.

Formulating the problem in the fin-plane avoids the need for computing the mode functions. The Green's function determined in Chapter 2 can be used, as it was in Chapter 3 for the moment method analysis. The author has investigated several iteration procedures which may be used in conjunction with such a formulation. This work involved a variant of the Spectral Iterative Technique (SIT) [29]. For guaranteed convergence, it would be advantageous to apply the conjugate gradient technique to this problem. These approaches are worthy of further consideration.

CHAPTER 5: DIELECTRIC WAVEGUIDE FILTERS

5.1. Introduction

Dielectric waveguide (DWG) filters are of particular interest for millimeter-wave end optical applications. A number of applications have been reported recently in the millimeter-wave and quasi-optical areas [30]-[32], and optical grating filters have been reported in [33]. Grating-type dielectric waveguide filters have several advantages over alternative configurations such as the ring-resonator filter [34], [35]. In particular, the ring resonator should be a number of wavelengths in circumference for satisfactory performance, which implies closely spaced spurious pass- or stop-bands. The filter can easily be incorporated into an integrated system and may be realized by a series of discontinuities such as surface or dielectric variations.

There has been some work done on mode-matching methods [36] in an effort to analyze discontinuities in a two-dimensional dielectric waveguide. It is difficult to apply these techniques to the analysis of grating filters considered in this chapter. It is proposed that a simple transmission line may be used to analyze such a grating structure. Experimentation has verified this approach. The theory developed is valid for a number of dielectric waveguide structures.

Section 5.2 gives details of the theoretical analysis of the dielectric waveguide grating filter. Experimental results are given in Section 5.3. Conclusions are outlined in Section 5.4.

5.2. Analysis of Dielectric Waveguide Grating Structure

A stepped dielectric grating structure and transmission line model are shown in Fig. 5.1. The waveguide known as image guide (rectangular dielectric guide on a ground plane) will be considered specifically, although the approach may be generalized to other dielectric waveguides. It is proposed that this model may be used for an approximate analysis of the grating filter.

The dielectric waveguide supports hybrid modes which may be expressed as a sum of longitudinal section electric (LSE) and longitudinal section magnetic (LSM) modes. The LSE fields may be expressed as [14]

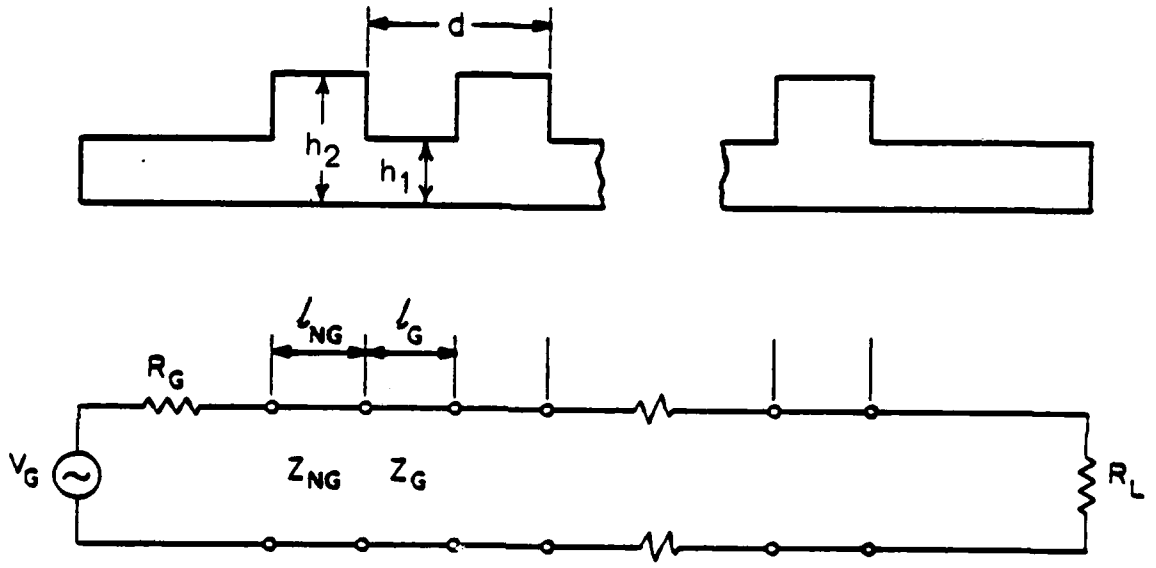

Figure 5.1. Image guide grating filter and transmission line model.

$$\overline{E} = -j\,\omega\,\mu\,\nabla \times \prod_h \tag{5.1a}$$

$$\overline{H} = \epsilon_r k_0^2 \prod_h + \nabla\,\nabla \cdot \prod_h \tag{5.1b}$$

and the LSM fields as

$$\overline{E} = k_0^2 \prod_e + \nabla(\epsilon_r^{-1}\,\nabla \cdot \prod_e) \tag{5.2a}$$

$$\overline{H} = j\,\omega\,\epsilon_0 \nabla \times \prod_e \tag{5.2b}$$

where $\prod_h$ and $\prod_e$ are the magnetic and electric Hertzian potentials, respectively.

With $\prod_h = \hat{y}\,\phi_h(x,y)e^{-j\beta z} = \hat{y}\phi_h$ and $\prod_e = \hat{y}\phi_e$ the dielectric waveguide fields may be expressed in terms of electric and magnetic scalar potential functions:

$$\begin{aligned}
E_x &= \frac{1}{\epsilon_r(y)}\,\frac{\partial^2\phi_e}{\partial x\,\partial y} + \omega\,\mu_0\beta\phi_h, \\
E_y &= \frac{1}{\epsilon_r(y)}\left[\beta^2\phi_e - \frac{\partial^2\phi_e}{\partial x^2}\right], \\
E_z &= -j\omega\mu_0\,\frac{\partial\phi_h}{\partial x} - \frac{j\beta}{\epsilon_r(y)}\,\frac{\partial\phi_e}{\partial y}, \\
H_x &= \frac{\partial^2\phi_h}{\partial x\,\partial y} - \omega\epsilon_0\beta\phi_e, \\
H_y &= \beta^2\phi_h - \frac{\partial^2\phi_h}{\partial x^2}, \\
H_z &= -j\beta\,\frac{\partial\phi_h}{\partial y} + j\omega\epsilon_0\,\frac{\partial\phi_e}{\partial x}.
\end{aligned} \tag{5.3}$$

The effective dielectric constant method [37], [38] is a very suitable approach for finding the propagation constant in planar dielectric waveguides. Various forms of dielectric waveguides may be analyzed in this manner. Consider the image guide structure of Fig. 5.2. Using the effective dielectric constant method and matching the fields in each region, the following eigenvalue equations may be found. The equation for k_y is

$$\epsilon_r\,\sqrt{k_0^2(\epsilon_r - 1) - k_y^2}\,\cos k_y y_1 - k_y \sin k_y y_1 = 0 \tag{5.4}$$

where ϵ_r is the relative permittivity of the guide. After solving for k_y, the effective dielectric con-

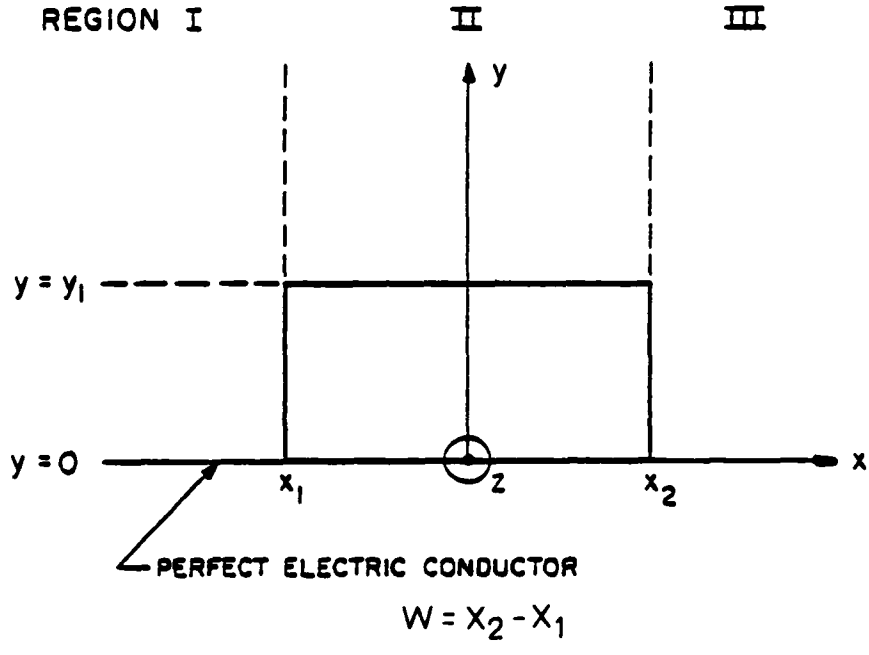

Figure 5.2. Image guide with coordinate system.

stant (ϵ_{e2}) for region 2 may be found:

$$\epsilon_{e2} = \epsilon_r - \frac{k_y^2}{k_0^2}. \tag{5.5}$$

The equation for k_x is

$$[k_0^2(\epsilon_{e2} - 1) - 2k_x^2]\sin k_x(x_2 - x_1) + \tag{5.6}$$
$$+ 2k_x\sqrt{k_0^2(\epsilon_{e2} - 1) - k_x^2}\cos k_x\,(x_2 - x_1) = 0.$$

Thus the guide propagation constant becomes

$$\beta = \sqrt{\epsilon_{e2}k_0^2 - k_x^2}. \tag{5.7}$$

The dominant mode will be considered in the following analysis. The waveguide characteristic impedance may be defined as

$$Z = \eta_0 \frac{k_0}{\beta} \tag{5.8}$$

where η_0, k_0 are the free-space wave impedance and propagation constant, respectively.

In order to find the filter transfer function, consider the unit cell shown in Fig. 5.3. The ABCD matrix for the unit cell may be obtained by multiplying the matrices for two line sections [39]. The unit cell matrix is

$$\begin{vmatrix} A & B \\ C & D \end{vmatrix}_1$$

$$A = \cos(\beta_G l_G)\cos(\beta_{NG} l_{NG}) - \frac{\beta_{NG}}{\beta_G}\sin(\beta_G l_G)\sin(\beta_{NG} l_{NG})$$

$$B = j\eta_0\left|\frac{k_0}{\beta_{NG}}\cos(\beta_G l_G)\sin(\beta_G l_G) + \frac{k_0}{\beta_G}\sin(\beta_G l_G)\cos(\beta_{NG} l_{NG})\right|$$

$$C = \frac{j}{\eta_0}\left|\frac{\beta_G}{k_0}\sin(\beta_G l_G)\cos(\beta_G l_{NG}) + \frac{\beta_{NG}}{k_0}\cos(\beta_G l_G)\sin(\beta_G l_{NG})\right| \tag{5.9}$$

$$D = \cos(\beta_G l_G)\cos(\beta_{NG} l_{NG}) - \frac{\beta_G}{\beta_G}\sin(\beta_G l_G)\sin(\beta_{NG} l_{NG}).$$

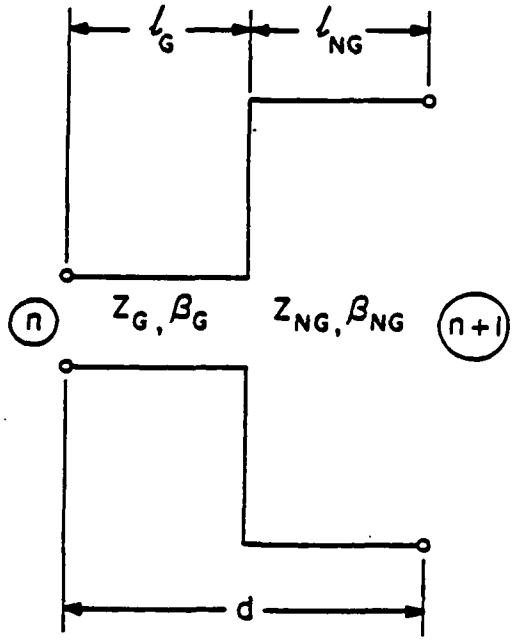

Figure 5.3. Unit cell in transmission line model.

The ABCD matrix for a grating structure of n unit cells is obtained by raising the matrix for a single cell to the nth power.

The transducer loss ratio is given by [39]

$$\frac{P_{avail}}{P_L} = \frac{1}{4R_G R_L}\left|(AR_L + DR_G)^2 + \left|\frac{B + CR_G R_L}{j}\right|^2\right| \tag{5.10}$$

where P_L is the power delivered to R_L and $P_{avail} = |V_g|^2/4R_G$ is the available power from the generator. This results in a method for computing the filter insertion loss (P_L/P_{avail}) as a function of frequency. Although this technique is approximate, the response predicted from such an analysis agrees well with measurements.

Fields in a periodic structure can be expressed in terms of spatial harmonics, according to Floquet's Theorem [19]. The propagation constants are

$$\beta_n = \beta_0 + \frac{2\pi n}{d},\ n = 0, \pm 1, \pm 2, \ldots \tag{5.11}$$

where d is the grating period. It is useful to look at the dispersion curves on a $k_0 d, \beta$ d-diagram, such as Fig. 3.6. Coupled mode theory may be used to explain the filter characteristics. There is a stop band when

$$\beta d = \pi \tag{5.12}$$

where β is the propagation constant in the grating. At this frequency there is coupling between the spatial harmonics $(\beta_0)_+$ and $(\beta_{01})_-$, which propagate in opposite directions. The waves are guided by the structure (slow-wave region). The grating exhibits a reflection coefficient close to one in the stop-band, and close to zero on either side.

Consider ports n and n+1 in the unit cell of Fig. 5.3, when the cell is part of an infinite periodic structure,

$$\begin{bmatrix} V_n \\ I_n \end{bmatrix} = \begin{bmatrix} A & B \\ C & D \end{bmatrix}\begin{bmatrix} V_{n+1} \\ I_{n+1} \end{bmatrix} = e^{\gamma d}\begin{bmatrix} V_{n+1} \\ I_{n+1} \end{bmatrix}. \tag{5.13}$$

For a lossless reciprocal network [40],

$$\cos \beta d = \frac{A + D}{2}. \tag{5.14}$$

The following relationship may thus be derived

$$\cos \beta d = \cos \beta_G l_G \cos \beta_{NG} (d - l_G) - \tag{5.15}$$

$$- \frac{1}{2} \left| \frac{\beta_G}{\beta_{NG}} + \frac{\beta_{NG}}{\beta_G} \right| \sin \beta_G l_G \sin \beta_{NG} (d - l_G).$$

For a particular d/l_G, the required d may be found from eq. (5.15) once the propagation constants β_G and β_{NG} for a uniform guide have been found from Eqs. (5.4)-(5.7).

5.3. Results and Discussion

Filter designs and response predictions were achieved using the procedures outlined in Section 5.2 with the aid of computer programs.

A scaled image-guide filter was built and tested in the X-band frequency range. The predicted and measured insertion loss responses and the dimensions are shown in Fig. 5.4. Rexolite 1422 was used as the dielectric, due to its favorable electrical and mechanical qualities. To enable testing with a network analyzer system, a suitable transition between metal waveguide and DWG is necessary. The transition used consists of a horn and an H-plane tapered section of DWG. This has been shown to act as a low-loss transition.

The predicted response is for matched loads at midband. (Maximum ripple across the band due to mismatch is less than 1 dB). Equation (5.14) predicts the lower edge of the stop-band, so a slight adjustment is necessary to obtain a required center frequency. The measurements agree quite well with predictions. Measured data in the 11 - 12 GHz range deviated from the predicted response. This deviation was due to radiation in this frequency range. It is generally accepted that grating-type slow-wave DWG structures have some inherent radiation problems. However, the radiation region may not cause a problem and could possibly be eliminated by tapering the steps at the ends of the structure [40]. Increasing the number of sections or the step size increases the stop-band insertion loss.

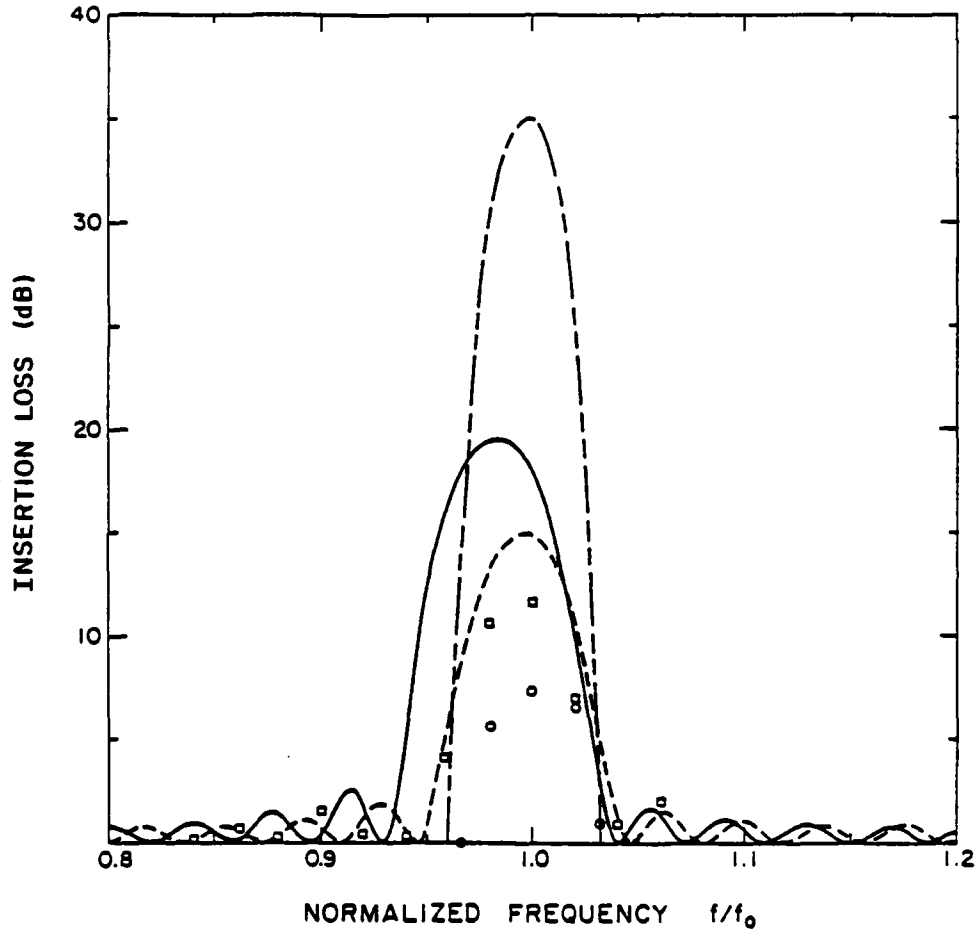

Figure 5.4. Predicted and measured insertion loss for grating filter. Rexolite 1422, $h_1 = 7\ mm$, $l_{NG}/d = 0.5$, $d = 11.2\ mm$, $f_0 = 10\ GHz$, $w = 20\ mm$.

Predicted:

——— $h_2 = 20\ mm$ } N=20 sections
– – – – – $h_2 = 14\ mm$ }

——— $h_2 = 14\ mm$ N=40 sections

Measured:

□ $h_2 = 20\ mm$ } N=20 sections
○ $h_2 = 14\ mm$ }

There are a number of interesting filter structures which employ gratings. These include:

(i) stagger-tuned grating sections in series to realize a low-pass or large stop-band band-reject filter (Fig. 5.5(a))

(ii) grating with coupler (Fig. 5.5(b)). The forward coupler action couples the reflected power from the grating to achieve a band-pass response between parts 1 and 2

(iii) tapering in the grating to obtain an equal-ripple response. The realizable β_G / β_{NG} limits this.

A simple yet effective means of analyzing dielectric waveguide grating filters has been presented. Experimentation has verified the theoretical analysis. This technique thus becomes a useful design tool which is applicable to many forms of periodic and non-periodic guided wave structures.

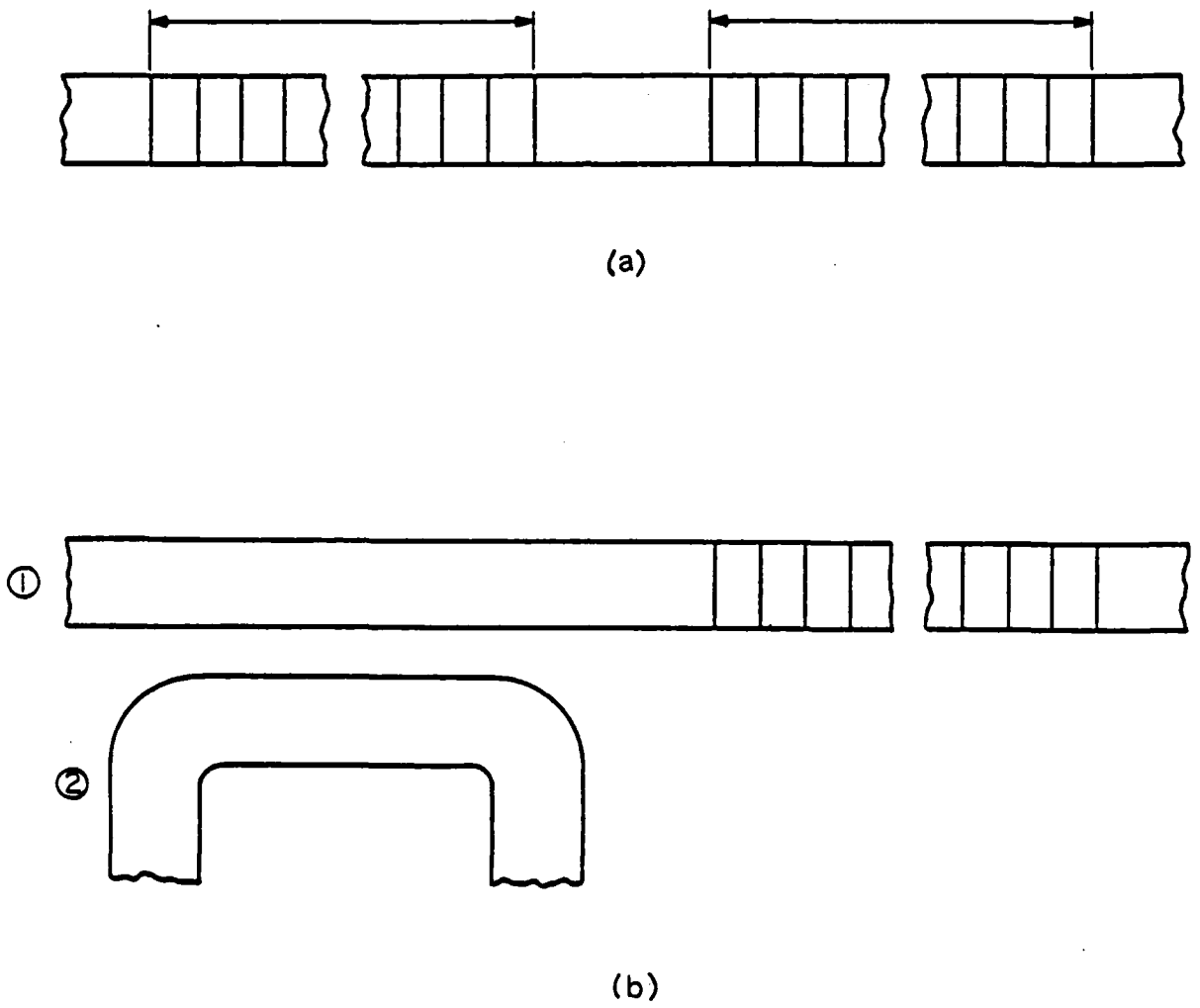

Figure 5.5. (a) Series stagger-tuned grating filter, (b) filter consisting of grating with coupler.

Chapter 6: CONCLUSION

Several millimeter-wave waveguide problems have been investigated. These problems involved a single or a series of discontinuities in fin-line and dielectric waveguide.

The uniform fin-line was analyzed in chapter 2. The problem was formulated in the spectral domain, and a numerical solution was obtained using the moment method. Results for the propagation constant, characteristic impedance and mode functions were given.

A two-dimensional spectral relationship in the plane of the metal fin was used to formulate the discontinuity problem in chapter 3. A single and an infinite periodic array of discontinuities were studied. The numerical solution was obtained by using a moment method. Results for the single discontinuity analysis and the dispersion curve for an infinite periodic array of discontinuities were given. In the case of the single discontinuity, efficient numerical evaluation of a number of integrals was important. Stability of the solution with respect to variations in the approximating functions was a problem.

In chapter 3 the fin-line discontinuity problem was formulated with unknowns in the transverse plane of the junction. Two numerical procedures were used to solve for these unknowns. The first, the conjugate gradient method, could solve the uniform problem well, but would not converge to the correct solution in the case of the discontinuity. The correct solution was not obtained because the number of degrees of freedom in the unknown was greater than the number of terms possible in the Green's function. The second approach involved a use of the generalized variational procedure, which represented the unknown in terms of characteristic functions. Satisfactory results were obtained with this approach.

A rectangular dielectric image guide grating filter was analyzed in chapter 5. The effective dielectric constant method in conjunction with a transmission line model was used. Satisfactory agreement between theory and experiment, for the insertion loss, was obtained.

REFERENCES

[1] "Special issue on solid-state, microwave/millimeter-wave power generation, amplification and control," *IEEE Trans. Microwave Theory Tech.*, vol. MTT-27, May 1979.

[2] "Special issue on microwave and millimeter-wave integrated circuits," *IEEE Trans. Microwave Theory Tech.*, vol. MTT-26, Oct. 1978.

[3] P. Meier, "Integrated fin-line millimeter components," *IEEE Trans. Microwave Theory Tech.*, vol. MTT-22, pp. 1209-1216, Dec. 1974.

[4] H. El Hennawy and K. Schunemann, "Computer-aided design of fin-line detectors, modulators and switches," *Arch. Elek. Ubertragung.*, vol. 36,pp. 49-56, Feb. 1982.

[5] F. Arndt, J. Bornemann, D. Grauerholz, and R. Vahldieck, "Theory and design of low-insertion loss fin-line filters," *IEEE Trans. Microwave Theory Tech.*, vol. MTT-30, pp. 155-162, Feb. 1982.

[6] Y. Shih, T. Itoh, and L. Bui, "Computer-aided design of millimeter-wave E-plane filters," *IEEE Trans. Microwave Theory Tech.*, vol. MTT-31, pp. 135-141, Feb. 1983.

[7] H. El Hennawy and K. Schunemann, "Hybrid fin-line matching structures," *IEEE Trans. Microwave Theory Tech.*, vol. MTT-30, pp. 2132-2138, Dec. 1982.

[8] J. Knorr and P. Shayda, "Millimeter wave fin-line characteristics," *IEEE Trans. Microwave Theory Tech.*, vol. MTT-28, no. 7, pp. 737-743, Jul. 1980.

[9] L. Schmidt and T. Itoh, "Spectral domain analysis of dominant and higher order modes in fin lines," *IEEE Trans. Microwave Theory Tech.*, vol. MTT-38, no. 9, pp. 981-985, Sep. 1980.

[10] L. Schmidt, T. Itoh, and H. Hofmann, "Characteristics of unilateral fin-line structures with arbitrarily located slots," *IEEE Trans. Microwave Theory Tech.*, vol. MTT-29, no. 4, pp. 352-355, Apr. 1981.

[11] J. BrianDavies and D. Mirshekar-Syahkal, "Spectral domain solution of arbitrary coplanar transmission line with multilayer substrate," *IEEE Trans. Microwave Theory Tech.*, pp. 143-146, Feb. 1977.

[12] T. Itoh, "Spectral domain immitance approch for dispersion characteristics of generalized printed transmission lines," *IEEE Trans. Microwave Theory Tech.*, vol. MTT-28, no. 7, pp. 733-736, Jul. 1980.

[13] R. Jansen, "Unified user-oriented computation of shielded, covered and open planar microwave and millimeter-wave transmission characteristics," *IEE Proc. Pt. H, Microwaves Opt. Acoust.*, vol. MOA 1, pp. 14-22, 1979.

[14] R. Collin, *Field Theory of Gudded waves.* New York, NY: McGraw-Hill, 1960.

[15] J. Wilson, "*Analysis of fin-line at millimeter wavelengths*," M.S. Thesis, University of Illinois, 1982.

[16] H. El Hennawy and K. Schunemann, "Impedance transformation in fin-lines," *IEE Proc. Pt. H, Microwaves Opt. Acoust.*, vol. 129, pp. 342-350, Dec. 1982.

[17] M. Helard, J. Citerne, O. Picon, and V. Fouad Hanna, "fin-line," *Electron. Lett.* vol. 19, pp. 537-539, 7th. Jul. 1983.

[18] T. Kitazawa and R. Mittra, "An investigation of striplines and finlines with periodic stubs," *IEEE Trans. Microwave Theory Tech.*, vol. MTT-32, pp. 684-688, Jul. 1984.

[19] R. Mittra and S. Lee, *Analytical Techniques in the Theory of Guided Waves.* New York, NY: Macmillan, 1971.

[20] R. Collin and F. Zucker, Eds., *Antenna Theory.* New York, NY: McGraw-Hill, 1969, Pt. 2, Chap. 19.

[21] P. Davis and P. Rabinowitz, *Methods of Numerical Integration.* New York, NY: Academic Press, 1975.

[22] W. Ko, V. Jamnejad, R. Mittra, and S. Lee, "Radiation from an open-ended waveguide with beam equalizer- a spectral domain analysis," *IEEE Trans. Antennas Propagat.*, vol. Ap-30, pp.44-52, Jan. 1982.

[23] H. Auda and R. Harrington, "A moment solution for waveguide junction problems," *IEEE Trans. Microwave Theory Tech.*, vol. MTT-31, pp. 515-519, Jul. 1983.

[24] R. Collin and F. Zucker, Eds., *Antenna Theory.* New York, NY: McGraw-Hill, 1969, Pt. 1, Chap 14.

[25] M. Hestenes and E. Stiefel, "Methods of conjugate gradients for solving linear systems," *Journal Res. Nat. Bur. Standards*, vol. 49, pp. 409-436, 1952.

[26] H. Schwarz, H. Rutishauser, and E. Stiefel, *Numerical Analysis of Symmetric Matrices.* Englewood Cliffs, NJ: Prentice Hall, 1973.

[27] P. Van Den Berg, "Iterative computational techniques in scattering based upon the integrated square error as criterion," *Proc. 1983 URSI Int. Symp. on Electromag. Thry.*, Spain, pp. 97-100, Aug. 1983.

[28] T. Sarkar, K. Siarkiewicz, and R. Stratton, "Survey of numerical methods for solution of large systems of linear equations for electromagnetic field problems," *IEEE Trans. Antennas Propagat.*, vol. Ap-29, pp. 847-854, Nov. 1981.

[29] C. Tsao and R. Mittra, "A spectral iteration approach for analyzing scattering from frequency selective surfaces," *IEEE Trans. Antennas Propagat.*, vol. Ap-30, pp. 303-308, Mar. 1983.

[30] T. Itoh, "Application of gratings in a dielectric waveguide for leaky-wave antennas and band-reject filters," *IEEE Trans. Microwave Theory Tech.*, vol. MTT-25, pp. 1134-1138, Dec. 1977.

[31] B. Song and T. Itoh, "Distributed bragg reflection dielectric waveguide oscillators," *IEEE Trans. Microwave Theory Tech.*, vol. MTT-27, pp. 1019-1022, Dec. 1979.

[32] T. Itoh and F. Hsu, "Distributed bragg reflector Gunn oscillators for dielectric millimeter-wave integrated circuits," *IEEE Trans. Microwave Theory Tech.*, vol. MTT-27, pp. 514-518 ,May 1979.

[33] R. Schmidt, D. Flanders, C. Shank, and R. Standley, "Narrow-band grating filters for thin-film optical waveguides," *Appl. Phys. Lett.*, vol. 25, pp. 651-652 Dec. 1974.

[34] J. Itanami and S. Shindo, "Channel dropping filter for millimeter-wave integrated circuits," *IEEE Trans. Microwave Theory Tech.*, vol. MTT-26, pp. 759-764, Oct. 1978.

[35] J. Kietzer, A. Kaurs, and B. Levin, "A V-band communication trasmitter and receiver system using dielectric waveguide integrated circuits," *IEEE Trans. Microwave Theory Tech.*, vol. MTT-24, pp. 797-803, Nov. 1976.

[36] T. Rozzi and B. In't Veld, "Field and network analysis of interacting step discontinuities in planar dielectric waveguides," *IEEE Trans. Microwave Theory Tech.*, vol. MTT-27, pp. 303-309, Apr. 1979.

[37] R. Knox and P. Toulios, "Integrated circuits for the millimeter through optical frequency range," *Symp. on Submillimeter Waves*, Polytechnic Institute of Brooklyn, NY, Mar. 31, 1970.

[38] W. McLevige, T. Itoh, and R. Mittra, "New waveguide sturctures for millimeter-wave and optical integrated circuits," *IEEE Trans. Microwave Theory Tech.*, vol. MTT-23, pp. 788-794, Oct. 1975.

[39'] G. Matthaei, L. Young, and E. Jones, *Microwave Filters, Impedance Matching Networks and Coupling Structures*. Dedham, MA: Artech House, 1980.

[40] R. Collin, *Foundations of Microwave Engineering*. New York, NY: McGraw-Hill, 1966, Ch. 8.

END

FILMED

1-86

DTIC